FLOW CONTROL OVER A CIRCULAR ARC AIRFOIL BY PERIODIC BLOWING

José M. Rullán

Thesis submitted to the Faculty of the
Virginia Polytechnic Institute and State University
in partial fulfillment of the requirements for the degree of

MASTER OF SCIENCE
In
Engineering Mechanics

Approved by

Demetri P. Telionis, Ph.D., Chair
Pavlos P. Vlachos, Ph.D., Member
Saad A. Ragab, Ph.D., Member

May 11, 2004

Blacksburg, Virginia

Keywords: Sharp edge airfoil, flow control, separated flow, jet pulsation, vortex formation

Flow control over a circular arc airfoil by periodic blowing

Jose M. Rullan

ABSTRACT

The flow over sharp-edged wings is almost always separated. The control of separated flows is possible and benefits can be achieved but only in a time average sense. A new design of an actuator was designed and tested which can achieve a wide range velocity of without frequency dependence, is free of oscillating components as well as free of secondary frequencies and therefore can be scaled up easily, unlike a traditional synthetic jet. The actuator can achieve a considerable amount of jet vectoring, thus aligning the disturbance with the leading edge shear layer.

Results indicate that unsteady mini-jet actuation is an effective actuation device capable of increasing the lift in the stall region of the airfoil. Moreover, pressure measurements showed that two parameters could be altered to maximize the lift. The momentum coefficient needed a minimum value to exert influence and the actuating frequency need not be at exact the natural shedding frequency to improve the lift and can be operated at harmonics of the natural shedding frequency and obtain improvements.

DEDICATION

To my family. Mari, you accepted my desire for this adventure and leave behind an already settled life. You are the one who always believe in me even when I do not. Miguel, you make opening the front door the most magnificent moment of any day.

ACKNOWLEDGEMENTS

I would like to express my deepest appreciation to my advisory committee. Dr. Demetri Telionis, you gave me the chance when you did not have to. Still you have always helped me and have look out for me. I would not be doing this great job that I enjoy if it were not for you. Dr. Pavlos Vlachos, your advice and your trust is always welcomed. I appreciate the patience and the help that you care to give me. And Dr. Saad Ragab, thanks for been always there when any question arises. A visit to your office is another class session.

Thanks to Dr. Matt Zeiger for all his ideas, input, and advice in this research. He always solved the problems and also found the time to be spent when he did not needed to. Also, I want to thank Robert Hodges for his time and ideas to work in the lab. I also appreciate the efforts and advice put on by the ESM Shop personnel. Both David Simmons and Darrel Link are extremely diligent.

To all my friends in the Fluids Lab, you made spending the days in the lab easier. I need to recognize Ali Etebari for always being helpful and at hand whenever work has to be done.

Last, to my family who are willing to sacrifice their time so I can do this fantastic work. You are the drive that pushes me in life.

TABLE OF CONTENTS

LIST OF FIGURES

LIST OF TABLES

NOMENCLATURE

α	Angle of attack
C_μ	Momentum Coefficient
U_∞	Freestream velocity
h	Slot width
c	airfoil chord
St	Strouhal number
F^+	Reduced frequency
$f_{shedding}$	Shedding frequency
$f_{actuator}$	Actuator frequency
Re	Reynolds number

1 INTRODUCTION

In recent years there has been an increased interest in the flow control field, especially in aerodynamics, with the purpose of increasing lift and decreasing drag of airfoils. Wings suffer from flow separation at high angles of attack due to viscous effects, which in turn causes a major decrease in lift and increase in drag. This occurs to all types of airfoils, but especially to sharp edge wings. These types of wings are used on supersonic transports as well as in stealth technology due to the fact that flat surfaces and sharp edges help reduce the radar signature of the airplane by reflecting the radar signals away from the radar, while also reducing the wave drag due to the shock wave that otherwise would be detached if round edge airfoils were used. The problems with these types of wing geometries are that they need long runways and require a lot of power for takeoff and landing since at subsonic flight the lift for these airfoils is reduced as well advanced control systems and highly skilled pilots to maintain a safe degree of maneuverability.

Sharp edge airfoils suffer from separation even at low angles of attack such as 8°, because the flow cannot negotiate the sharp turn at the leading edge. As the flow separates, the airfoil behaves as a bluff body. Due to this separation, a reduction in lift will be experienced by the airfoil due to the fact that the airflow on the suction side of the airfoil is separated and vortex shedding starts. The interest in this study is to try to control separated flow, not flow separation. With the implementation of flow control techniques, improvements in the lift coefficient can be obtained in a time-averaged sense. This is achieved by controlling the vortex-shedding phenomenon that in turn will improve a mixing enhancement of high momentum flow from the free stream with low momentum flow in the separated region. This mechanism is known as vortex lift.

1.1 Separated flow

As stated before, the purpose of this research is to control separated flow and not flow separation. It is important to make this distinction, since the former refers to the effort of working along with a flow field that has already experienced boundary layer separation from a wall while the latter tries to prevent or delay separation, or reattach the

flow field. Fiedler et al (1998) classified flow separation and possible techniques to address their situation as shown in Figure 1-1.

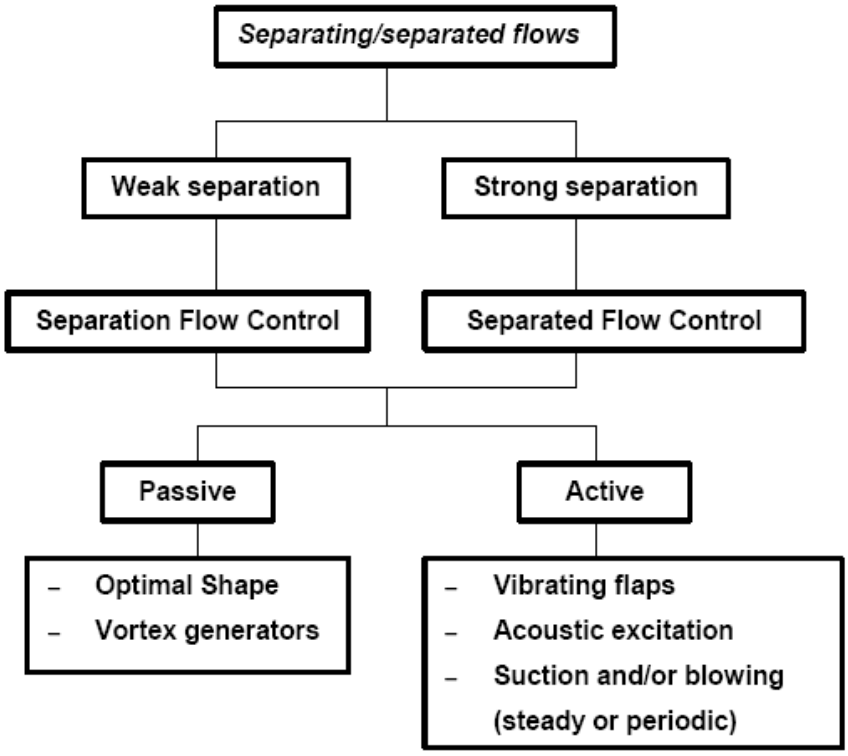

Figure 1-1: Classification of flow field separation and flow management techniques

Viscous flow theory predicts that a boundary layer forms on a wall due to viscosity forces where there is going to be a substantial variation of the velocity across the streamlines. It also states that a flow will separate in the presence of an adverse pressure gradient. For sharp edge airfoils, separation will always be fixed at the sharp leading edge since separation will occur at sharp corners due to the adverse pressure gradient. Sharp edge airfoils will suffer from massive separation at around eight degrees angle of attack.

When the flow separates from the wall, the boundary layer theory no longer holds since a shear layer will be formed. Vortices will be formed and they will be shed from the separation points located at the leading and trailing edges in an alternate way. These vortices are energized by the interaction of each other so the ones that are shed from the leading edge are in a disadvantage since these leading edge vortices are very weak to accomplish formation (Roshko 1967) so they may form or not until they reach the wake. This research will try to accomplish the enhancement of the leading edge vortices to see

if they roll over the suction side surface thus obtaining a lower pressure and increasing the lift. We need to lay out the physical mechanism of the production, shedding, capture and enhancement of these vortices at post-stall angles of attack. Wu et al (1991) summarizes these four steps of the physics as vortex layer instability-receptivity-resonance.

When flow separates, the result is the continuous shedding of a free shear layer. This shear layer, a vortex layer in itself, is unstable to small perturbations (Kelvin-Helmholtz instabilities) and the instabilities will cause a vortex merging. The upstream layer instability induces stronger and coherent vortex merging downstream (Ho et al 1984) as sketched in Figure 1-2. This encouragement is repeated thus doubling the size of these global instabilities each time. This interaction of the shear layer with itself is called a feedback mechanism.

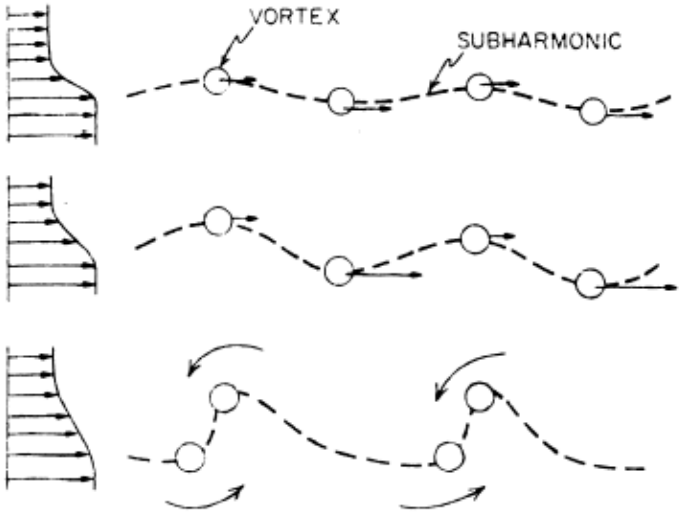

Figure 1-2: Vortex induction by instabilities in a free shear layer.

It is important not only to understand the vortex layer evolution but its resonance as well. Resonance can best be described from oscillation theory. If a forcing term matches one of the fundamental modes of a linear oscillator then a magnified response will develop and the oscillator's response will be amplified. Even some higher order modes might be amplified and manage somewhat this vortex flow.

Resonance needs the interaction of two periodic events that are in phase with frequencies that are integer multiples of each other. For this to occur a periodic flow feature and a feedback mechanism are needed so the disturbance enables the layer to

interact with itself. The purpose is to trigger a self-organizing mechanism of relative small energy input so that the energy is drawn from the random fluctuating motion or vorticity concentration such as the ones produced by mechanical flaps and unsteady jets. Here the vortex shedding frequency is locked and also must of the energy is converted into the vortex itself. The problem vortex-vortex interaction is that the frequency range is usually up to 100 Hz. A good feature is that the forcing frequency does not need to be the optimal resonance frequency to achieve a significant effect.

1.2 Flow control

Flow control is defined by Gad-el-Hak (2001) as the ability to actively or passively manipulate a flow field to effect a desired change. The challenge is to achieve that change with a simple device that is inexpensive to build as well as to operate and has minimum side effects. Control of separated flow is possible by both passive and active means as presented in Figure 1-3. Passive control refers to the ones that require no auxiliary power and no control loop and sometimes are referred as flow management rather than control. Examples include changing the geometry of the aircraft to increase its aerodynamic properties such as wings equipped with leading edge flaps. These are heavy, require extra hydraulic control and introduce serious problems to sustain the stealth integrity of the aircraft. This type of control is unacceptable in the present case, due to stealth geometry and speed constraints.

On the other hand active flow control refers to the ones where a control loop is used and energy expenditure is required. They are also further divided into predetermined and reactive. Predetermined control loops refer to the application of steady or unsteady energy without regard to the particular state of the flow so no sensors are required. This is the difference with the reactive ones since these employ a sensor to continuously adjust the controller. These reactive ones in turn could be either feedforward or feedback controlled. In the present research, we employ a predetermined loop control.

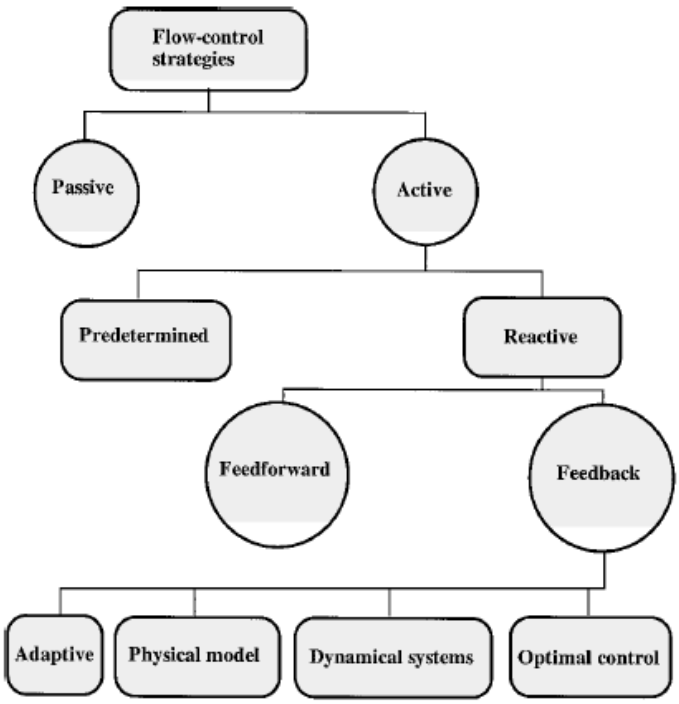

Figure 1-3: Classification of flow control methods.

1.2.1 Mechanical Flaps

Zhou et al (1993) were the first to try to do control on a sharp edge airfoil. They used a rounded edge airfoil placed backwards in a wind tunnel so the sharp trailing edge faced the oncoming flow. Their test was only at 27° angle of attack but their results indicated that an increase in lift could be achieved.

Hsiao et al (1993) employed a pulsed micro-flap on the leading edge of a wing to control separated flow. They focused on the position, amplitude, and frequency of the flap motion necessary to improve the aerodynamics characteristics of the flow over an airfoil at high angles of attack. Hsiao and Wang found that periodic perturbations can organize and enhance the average strength of the shedding vortices and can increase in a time-average sense the lift by as much as 50%. Hsiao et al (1998) later made modifications to their previous design, finding that the most effective excitation corresponds to a flap motion with the vortex shedding frequency. They also found that larger amplitudes of excitation motion produced a larger lift coefficient.

In order to create the necessary flow disturbance, Miranda (2001) used a small oscillating flap placed on the leading edge of a circular arc sharp-edged airfoil. This pulsing flap creates an unsteady excitation at the leading edge, which is responsible for

affecting the flow in the desired way. They showed an increased in lift of up to 70%. Previous work has demonstrated that the maximum effect on separated flow can be achieved when the actuation frequency is near the vortex shedding frequency. But the flap must penetrate the separated region in order to have any effect on the formation of vortices. That is the reason suggested since the effect was greatly reduced as the angle of attack was increased. They also found that oscillating flaps are not limited in their frequency domain. Indeed, they demonstrated that an oscillating flap could generate a wide range of effective frequencies for the control of separated flow over a sharp-edged airfoil. But such devices may not be attractive to the aircraft designer.

1.2.2 Periodic blowing

A blowing technique has also been tested to control separated flow. Small jets are mounted at the leading edge of airfoils for the purpose of developing periodic perturbations into the boundary layer. The idea is to produce streamwise vortices using transverse steady and oscillating flow jets to increase the cross-stream mixing and lead to stall suppression in adverse pressure gradients. Several studies have been conducted on the use of oscillating blowing. McManus and Magill (1996) studied the separation control in incompressible and compressible flow using pulsed jets. They tested a NACA-4412 airfoil section with a leading-edge flap. The leading-edge flap was fitted with flow control actuators, each actuator consisted of a cross flow jet with pitch and screw angles of 90 and 45 degrees respectively. High-speed flow control valves were used to control the pulsed flow to each jet individually. The leading edge contained three jet nozzles; however only two were used. The valve open-and-close cycle was manipulated using a computer function generator driving a solenoid valve power supply. The valve controller allowed pulse rates up to 500 Hz and volume flow rates in excess of 20 slugs/min for each jet. A constant average mass flow of air was supplied to the jet using a closed-loop servo valve. Their data indicated that maximum lift enhancements occur with a jet pulse Strouhal number of approximately 0.6. However, McManus and Magill found the pulsed jets caused an increase in lift of up to 50 percent over a base line case for $\alpha \leq 10$ degrees. It was found that the effectiveness decreased with the increase in Mach number. The best results were found when the angle of attack was equal to the angle corresponding to C_{lmax}.

Seifert et al (1993) examined oscillatory blowing on the trailing edge flap of a NACA-0015 airfoil. They activated jets mounted in a 2-D slot located on the upper surface above the hinge of the flap. The airfoil was placed at an angle of attack of 20 degrees. Seifert et al. concluded that steady blowing had no effect on lift or drag. However, modulating blowing generated an increase in lift and cut the drag in half.

Synthetic-jet actuators can be used effectively achieve dynamic blowing and suction. Synthetic-jet actuators based on piezoelectric devices are most efficient at the resonance frequency of the device and limited by the natural frequency of the cavity. Such actuators have proven very useful in the laboratory but may not be as effective in practice. Rao et al (2000) designed an actuator, which is essentially a small positive-displacement machine. The same group later designed a similar device and tested a NACA0015 airfoil with rounded leading edges containing six reciprocating compressors, which were driven by two DC motors. These compressors/pistons created a synthetic jet (zero mean flux) at the leading edge of the airfoil. They found that flow separation control was demonstrated at angles of attack and free stream velocities as high as 25° and 45 m/s, respectively. These actuators may have overcome some of the problems faced by other designs but they are complex machines, requiring high-speed linear oscillatory motions and complex mechanical components.

1.2.3 Other actuations

There are other devices tried for active flow control and could be applied to post-stall flow control. Among some recent technology, one of the most talked about in general is piezoresistors. Jacobson et al (1997) designed an actuator that consists of a piezoelectrically-driven cantilever mounted flush with the flow wall and could be used in large arrays for actively controlling transitional and turbulent boundary layers. When driven, the resulting flow disturbance over the actuator is a quasi-steady pair of counter-rotating streamwise vortices with strengths controlled by the amplitude of the actuator drive signal. These vortices decay rapidly downstream of the actuator but they produce a set of high- and low-speed streaks that persist far downstream. Piezoelectric actuators are also mechanical such as the one by Cattafesta et al (2001), where one sheet of piezoceramic was attached to the underside of a shime. Here the actuator works as a flap and is able to produce significant velocity fluctuations even in relative thick boundary layers.

Another type of actuators considered are called electrohydrodynamic, introduced by Artana et al (2002) where flush mounted electrodes in a flat plate with a DC power supply are used to create a plasma sheet. This plasma sheet seems to induce an acceleration in the flow close to surface thereby increasing its momentum and inducing a faster reattachment as seen in the flow visualization.

1.3 Methodology

So far, efforts have been reported to control the flow separation over airfoils with rounded leading edges, while here we report on the control of separated flow over sharp-edged airfoils. These techniques are equally applicable for the control of separated flows over rounded airfoils. There are two important differences between the actuator requirements for the two cases. First, the location of the actuators for the control of separation over rounded airfoils is not critical since the flow is still receptive to an external disturbance, whereas for the control of separated flow the actuation must interact with the free-shear layer. This fact dictates that the actuator of a sharp-edged wing must be as close as possible to the sharp edge, which leads to the second important difference. The direction of the actuation disturbance must be adjusted to lead the disturbance as much as possible in the direction of the free shear layer. Two additional important parameters are the momentum coefficient C_μ and frequency of the actuation. Different angles of attack and free stream velocities will require a wide variety of possible combinations. Been able to independently control both is a great challenge. These requirements may appear too stringent for the sharp- edged airfoils but on the other hand, they may provide some opportunities for robust control with minimal energy input. It is possible that free shear layers would be more receptive to disturbances right at their initiation that is as close as possible to the sharp leading edge. Another similar situation is the control of asymmetric wakes over pointed bodies of revolution at incidence. In this case, minute disturbances very close to the apex can feed into the global instability of the flow and lead to very large wake asymmetries as shown by Zilliac et al (1990) and Zeiger et al (1997).

It is important to note that periodic blowing is more effective than a steady jet due to resonance. For blowing, the momentum coefficient is define by McCormick (2000) as

$$C_\mu = \frac{\left(\rho h u^2\right)_{jet}}{\left(\rho c U^2\right)_\infty}$$

where ρ is the density of air and cancels out, h is the slot height, c is the chord of the airfoil and u and U are the respective velocities of the jet and the free stream. This is the relation of the input energy to kinetic energy of the free stream and is suggested in Wu et al (1997) that it should to be at least 1%.

The disturbance frequency likely to be amplify the most is given, using linear stability theory, by the Strouhal number $St = \frac{f_{shedding} \times c \times Sin(\alpha)}{U_\infty}$ where $f_{shedding}$ is the shedding frequency, c is the airfoil chord, α is the angle of attack and U_∞ is the free stream velocity. We are going to assume a value of $St=0.2$ for this research as is thoroughly accepted in literature. Seifert et al (1999) gives the actuation frequency, related to the shedding frequency, the reduced non-dimensional frequency $F^+ = \frac{f_{actuation}}{f_{shedding}}$. He suggests that this reduced frequency to be $0.4 < F^+ < 2$ since it seems that harmonics play a role in the dynamic process.

2 EXPERIMENTAL SETUP AND EQUIPMENT

2.1 Introduction

Measurements were carried out in two wind tunnels and a water tunnel. The water tunnel and the small wind tunnel are located in the ESM fluids laboratory at Norris Hall. The other wind tunnel is the Stability tunnel located in Randolph Hall. Two different models were constructed: one for air pressure measurements in the wind tunnel and another for flow visualization and velocity measurements in the water tunnel. The facilities and the models are here briefly described.

2.2 Wind tunnels

2.2.1 ESM wind tunnel

The ESM wind tunnel is an open-circuit, low-speed tunnel constructed in 1983. To reduce the turbulence level one honeycomb and four nylon-conditioning screens are included in the settling chamber. A five-to-one contraction follows the settling chamber. The test section dimensions are 51 cm x 51 cm x 125 cm (20 in x 20 in x 50 in) and include a removable plexiglass wall for easy access as well as visualization. The tunnel is powered by a 15 hp motor. Adjusting the relative diameters of the drive pulleys sets the tunnel speed. It can achieve free-stream velocities from 4 m/s to 35 m/s. The turbulence level does not exceed 0.51% at a free-stream velocity of 10 m/s, except for regions very near the tunnel walls. The flow across the test section has a velocity variation of less than 2.5%. Figure 2-1 shows a schematic of the wind tunnel.

The tunnel free stream velocity is obtained by a Pitot tube mounted on one of the side walls, which is connected to the data acquisition system as well as a Edwards-Datametrics Barocel precision transducer model 590D-100T-3Q8-H5X-4D and this in turn was connected to a 1450 Electronic Manometer that would provide a readout of the dynamic pressure. The Barocel has a range of 0-100 Torr with an accuracy of 0.05% of the pressure reading and a full-scale resolution of 0.001% .

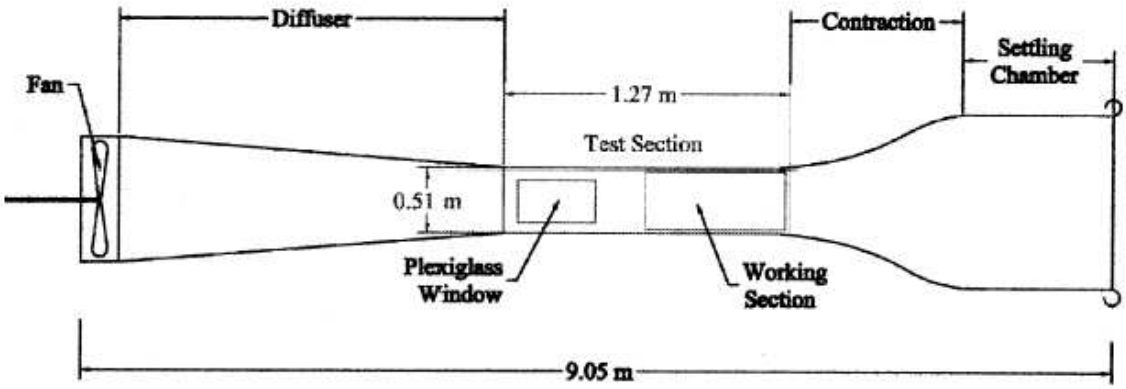

Figure 2-1: ESM Wind Tunnel Schematic

2.2.2 Virginia Tech Stability wind tunnel

The Virginia Tech Stability wind tunnel is a continuous, closed-loop subsonic wind tunnel. The maximum achievable flow speed is 275 ft/s (83.8 m/s) in a 6-foot by 6-foot by 25-foot (1.83m×1.83m×7.62m) test section. This facility was constructed in 1940 at the present site of NASA Langley Research Center by NASA's forerunner, NACA. Use of the tunnel at Langley in the determination of aerodynamic stability derivatives lead to its current name. In 1959, the tunnel was moved to Virginia Tech where it has been located outside of Randolph Hall.

The settling chamber has a contraction ratio of 9 to 1 and is equipped with anti-turbulence screens. This combination provides an extremely smooth flow in the test section. The turbulence levels vary from 0.018% to 0.5% and flow angularities are limited to 2° maximum. The settling chamber is 3m long and the diffuser has an angle of 3°. The ambient temperature and pressure in the test section is nearly equal to the ambient outdoor conditions due to the presence of a heat exchanger. During testing the control, room is maintained at the same static pressure as the test section. The tunnel fan has a 14-foot (4.27m) diameter and is driven by a 600 hp motor. Shows an schematic of the Stability tunnel.

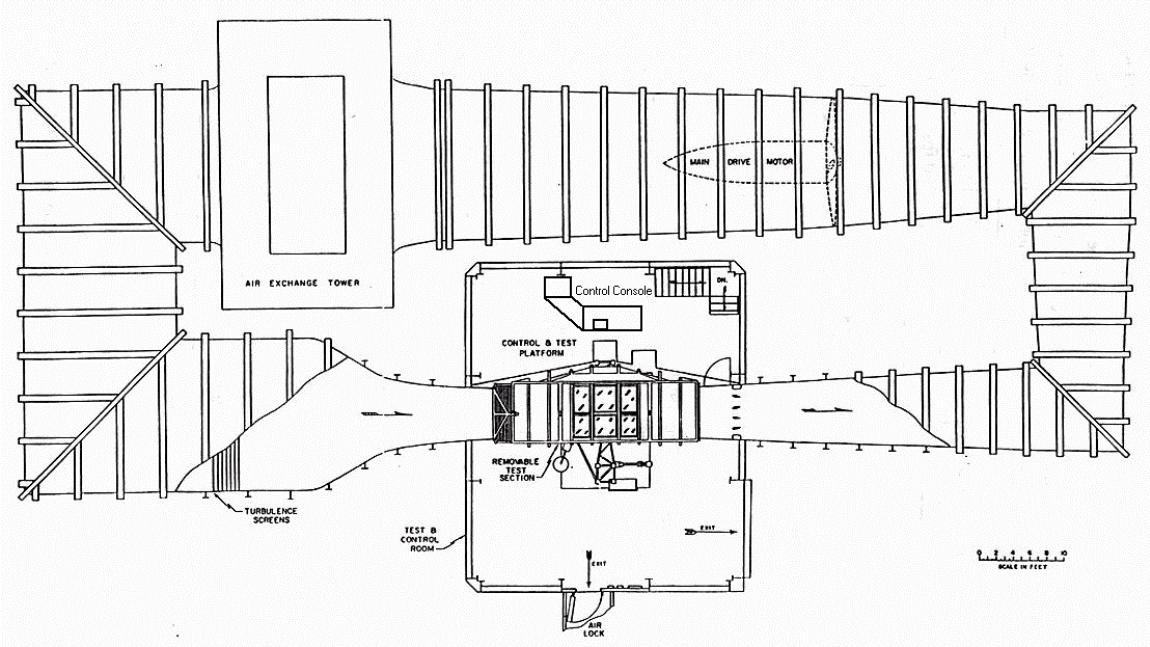

Figure 2-2: Stability tunnel schematic

2.3 Wind tunnel experimental rig

2.3.1 Model

The model used for this phase is a symmetric circular arc 12 ½ percent chord thickness airfoil. The chord length is 16 in with a resulting maximum thickness of 2 in. Its span is 20 in. It was built in two separate phases: the jet actuator and leading edge and the body of the airfoil.

The design of the jet mechanism took into account the desire of having it as close as possible to the leading edge of the airfoil. The leading edge part of the wing is essentially a wedge prism as shown in

Figure 2-3. The actuation mechanism consists of two concentric cylindrical surfaces as shown in Figure 2-4. The inner cylinder is a 7/16”-diameter inner brass tube that contains eight 1/16” wide slots and 1 ½ “long with 1/16 separation between them. The inner cylinder rotates about a fixed axis inside a fixed outer cylindrical surface created by the machined wedge. The inner cylinder is a brass tube, free to rotate on three bushings. One bushing was machined to fit snugly between the brass tubing and the machined leading edge at mid-span. This was done to eliminate possible warping of the tube during rotation.

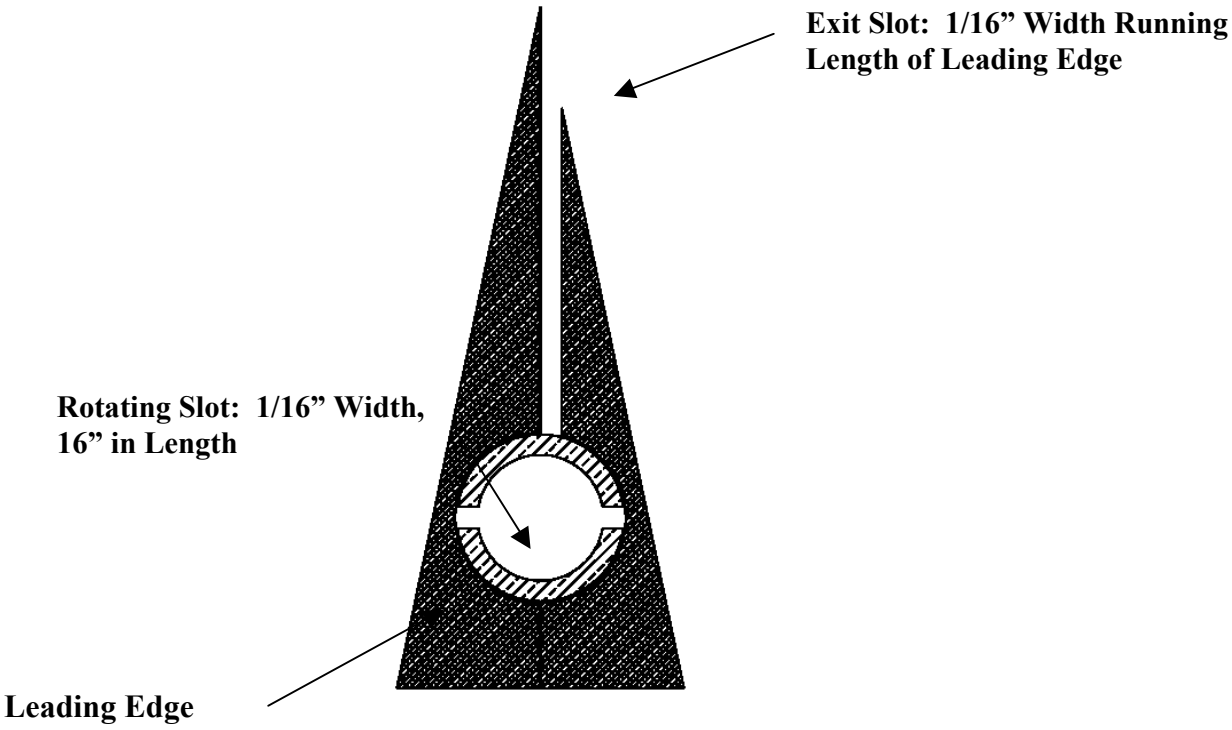

Figure 2-3: Leading Edge Cross Section

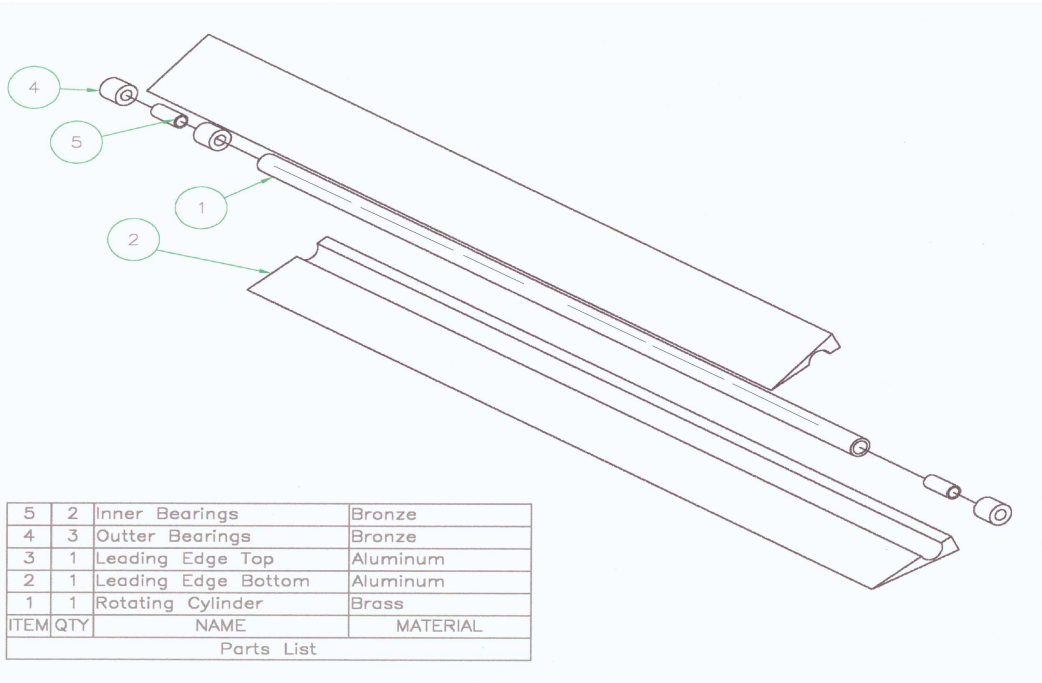

ITEM	QTY	NAME	MATERIAL
5	2	Inner Bearings	Bronze
4	3	Outter Bearings	Bronze
3	1	Leading Edge Top	Aluminum
2	1	Leading Edge Bottom	Aluminum
1	1	Rotating Cylinder	Brass

Parts List

Figure 2-4: Exploded View of Leading Edge and Flow Control Device

The body was made entirely of aluminum and consists of three holding ribs and two 1/32 sheets that serve as the skin. The ribs have holes through them that provide access to the inside.

Each side has 32 pressure taps aligned and located at 177.8 mm (7 in) from starboard side as can be seen in Figure 2-5. The taps start at 63.5 mm (2 ½ “) from the leading edge and are spaced at 10.16 mm (0.4 in) along the arc. Stainless steel tubing of 1.27 mm (0.05 in) o.d., 0.8382 mm (0.033 in) i.d. and 6.35 mm (1/4 in) in length was inserted in each tap with tygon tubing R-3603 of 2.38125 mm (3/32 in) o.d. and 0.79375 mm (1/32 in) i.d. connecting them to the pressure transducers.

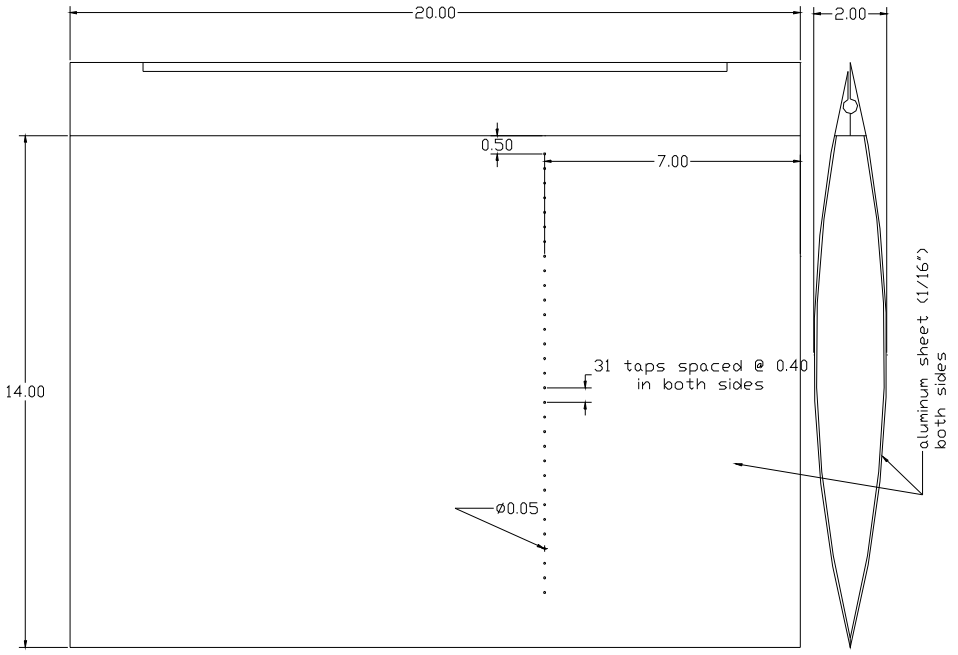

Figure 2-5: Wind tunnel model

To evaluate the capabilities of the actuator, the assembled leading edge actuator along with a rake of high-frequency-response Pitot tubes were mounted, as shown in Figure 2-6. Endevco model 8510 pressure transducers were used as sensing elements inside the rake. The output of the pressure transducers was connected to a HP digital signal analyzer, which was used to measure jet frequencies. In addition, these were also connected to a simple PC-driven 12-bit data acquisition system. The rake was mounted on traversing scales so it could easily be displaced to obtain data at different locations relative to the slotted nozzle.

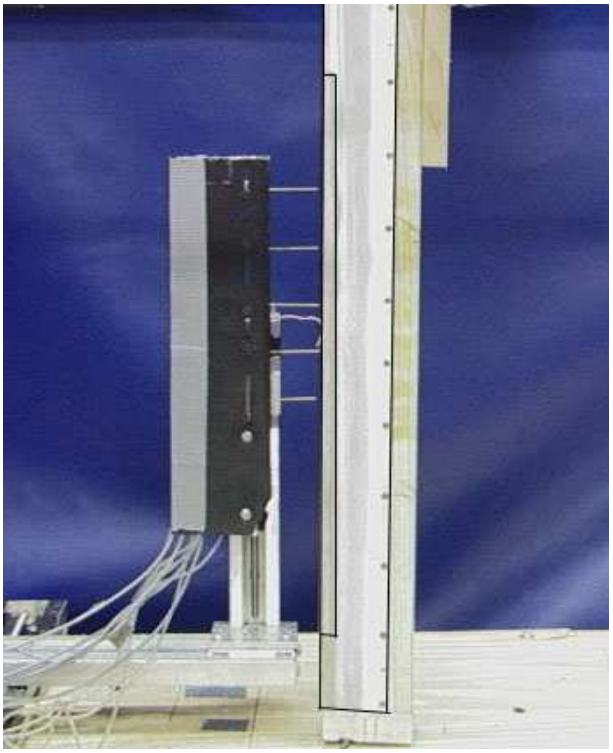

Figure 2-6: Leading Edge Aligned with Pitot Rake

2.3.2 Data Acquisition system

The pressure transducers used here are Pressure Systems Inc. ESP pressure scanners. These scanners are small, high-density packages containing multiple differential sensors. Two 32 channel scanners were used here, one with 10" of water range and the other with 20" of water range. Each channel is a mini piezoresistive pressure transducer and their output is internally amplified to ±5V full scale. These transducers have an accuracy of 0.10% of full scale after full calibration and a frequency response of 50 Hz. The transducers are differential and the reference pressure taken was the free stream static pressure. The last port in the second ESP was set aside for the tunnel total pressure to obtain the free stream velocity.

Pressure data were acquired using the ESP scanners that were mounted inside the model. The ESP's were connected to dedicated boards for digital addressing as well as voltage regulation. Since the ESP's have a maximum frequency response of 50 Hz they were sampled at 250 Hz and the sampling was done by a data acquisition board from Computer Boards model CIO-DAS08 12-bit A-D converter installed on a 233 MHz Pentium II processor installed computer. The Endevco pressure transducers were

connected to the same setup system although their inputs are acquired as external sources. They were calibrated properly.

This system was developed in house and has proprietary software as well as physical setup. For more detailed information on this data acquisition system the reader is referred to Zeiger (2003).

2.4 Water Tunnel

The ESM Water Tunnel was designed and built by Engineering Laboratory Design (ELD). The system is a closed loop design with the flow arranged in a vertical configuration with an approximate capacity of 9463 liters (2500 gallons) of water. An schematic is provided in figure Among the tunnel components are the flow sections, that includes a return plenum with turning system that divides and directs the flow after the test section, 24 inches return PVC pipe, an inlet plenum, a flow straightener and a three-way contraction convergence. The test section is a 61 cm x 61 cm x 183 cm (24" x 24" x 72") made out of a 1 ¼ inch clear acrylic plexiglass and a removable top that was not used during the present work. The final components of interest are a 17000 liters/min (4500 GPM) single stage pump and a variable speed drive assembly that consist of a 15 kW (20 hp) AC motor and a variable frequency controller that allows for a range of flow velocities in the test section from 3 cm/s (0.1 ft/s) to 50 cm/s (1.5 ft/s).

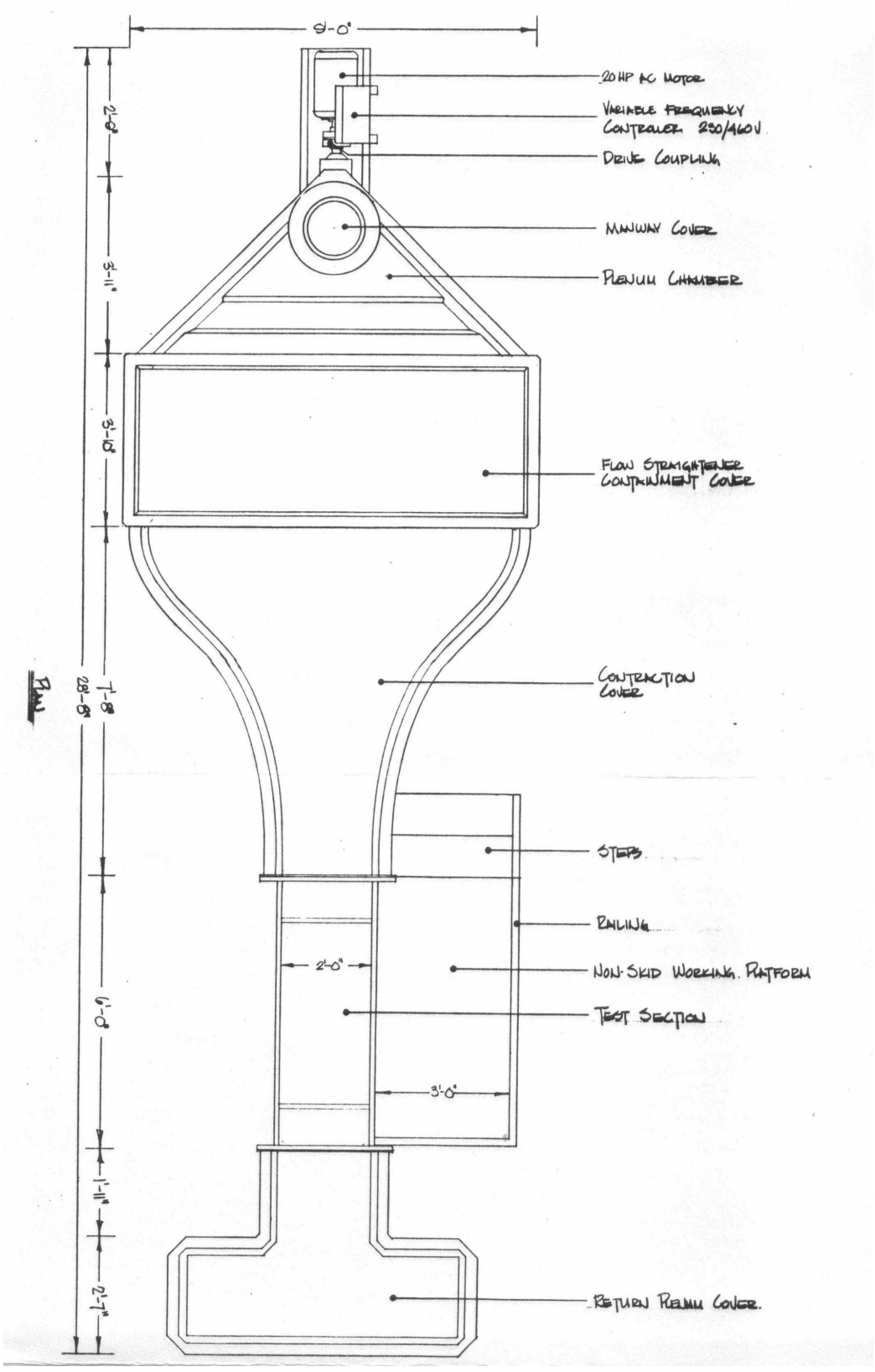

Figure 2-7: ESM Water tunnel Schematic

2.5 Water Tunnel Model

A first generation water tunnel Sharp Edge Airfoil model has been designed and fabricated out of ABS plastic using a rapid-prototyping facility. This model is shown in Figure 2-8. Its internal chamber is connected with high precision, computer-controlled gear pumps via the water supply connector shown in the same figure. The pumps allow the generation of pulsing jets with non-zero mean flow, or synthetic jet actuation via blowing and suction action. The airfoil section is geometrically similar to the one fabricated for the wind-tunnel tests. The chord was 100 mm and the maximum thickness was approximately 15% of the chord. The span of the model was 220 mm while a uniform jet-exit slot with 1mm width was placed within 5% from the leading edge. Finally, end plates were installed at the tips of the model in order to assure two-dimensional flow and control of the end effects.

For the experimental results presented here, the Reynolds number based on the chord was Re=25,000. The airfoil was placed at an AOA=25 deg in order to generate a massively separated flow. Based on a Strouhal number of 0.2 the natural shedding frequency was estimated around 1Hz. The latter was chosen as the actuator frequency yielding F^{+}=1. The actuator pulsed as a positive net-mass flow actuator with zero offset and an amplitude of u_{jet}=0.15m/s with 50% duty cycle. The above numbers result in a $C\mu$=0.006. Three cases will be presented here. First the flow of the pulsing jet alone, second the flow over the airfoil with no control and finally the flow with the control. These cases were investigated using two different magnifications, first with the field of view covering the whole airfoil with 1 mm spatial resolution, and then with fine resolution of 0.5 mm zooming near the actuator jet.

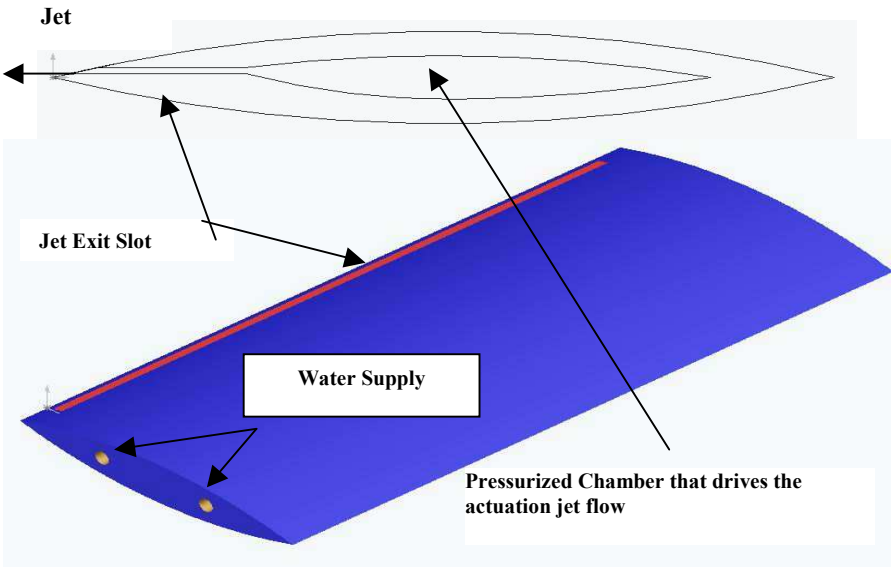

Figure 2-8: Water tunnel model

2.6 Particle Image Velocimetry System

This is a facility equipped with state of the art, in-house developed Time Resolved Digital Particle Image Velocimetry (TRDPIV). This PIV system is based on an Oxford Systems powerful laser (55 Watts), which is guided through a series of special mirrors and lenses to the area of interest and is opened up to a laser sheet directed across the field as shown in Figure 2-9. For the research conducted here, the laser sheet was placed in the mid-span of the airfoil aligned parallel to the free-stream. The free stream velocity was 0.25 m/s with corresponding water tunnel free stream turbulence intensity approximately 1%. A traversing system allows adjusting the distance from the models to the laser sheet. The flow is seeded with neutrally buoyant fluorescent particles, which serve as flow tracers. The diameter of the particles is on the order of 100 microns such that the particles accurately follow the flow with no response-lag to any turbulent fluctuations. A CMOS video camera captures the instantaneous positions of the particles. The laser and the camera are synchronized to operate in dual frame single exposure DPIV mode with sampling frequencies of 1000 Hz. This mode of operation allows very detailed temporal resolution, sufficient for resolving the turbulent flow fluctuations present in the wake.

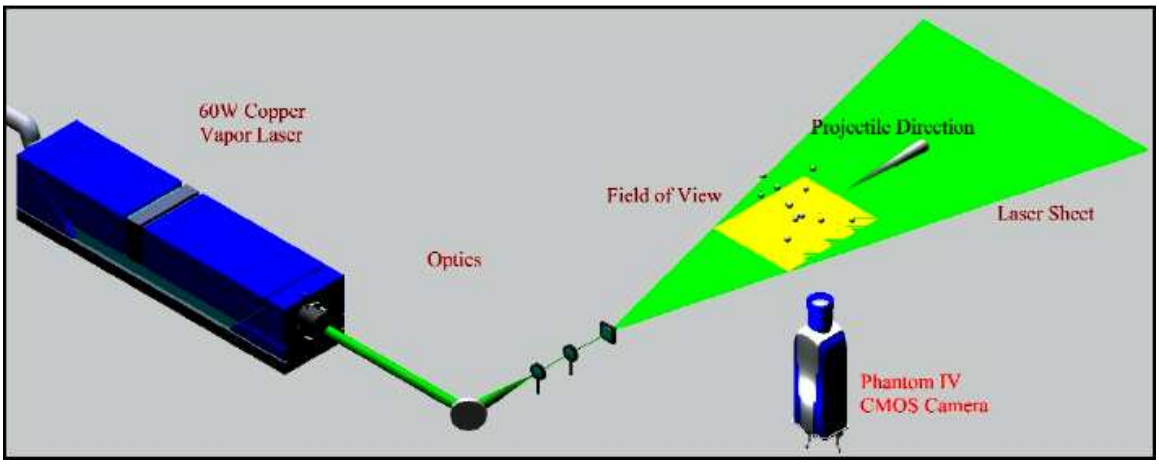

Figure 2-9: Schematic of experimental setup, which includes a 55-Watt Cu-Vapor pulsing laser, a high speed CMOS camera, optical lenses, and the flow field.

The velocity evaluation is carried out using a multi-grid iterative DPIV analysis. The algorithm is based on the work by Scarano and Rieuthmuller. In addition to their method we incorporated a second-order Discrete Window Offset (DWO) as proposed by Wereley and Meinhart. This is a simple but essential component. Time-resolved DPIV systems are limited by the fact that the time separation between consecutive frames is the reciprocal of the frame rate, thus on the order of milliseconds. This value is relatively large compared with microsecond time-intervals employed by conventional DPIV systems. By employing a second order DWO we provide an improved predictor for the particle pattern matching between the subsequent iterations. Moreover, the algorithm employed performs a localized cross-correlation which, based on our preliminary work, when compared to standard multi-grid schemes for resolving strong vortical flows was proven to be superior. Further details on the system, the algorithm and the associated error analysis can be found in Abiven et al (2002).

For the needs of the present study, the multigrid scheme was employed with a window hierarchy of 32-32-16-16-8 pixel2 and a space resolution of 4 pixel/vector. Two different magnifications were employed resulting in 0.5 mm and 1mm space resolution. The overall performance of the method yield time resolution 1 milliseconds with sampling time up to 2 secs. and average uncertainty of the velocity measurement on the order of 10-3 m/s independently of the velocity magnitude. The vorticity distribution in the wake is calculated from the measured velocities using 4th order, compact, finite-difference schemes 16.

3 JET CHARACTERIZATION

A thorough understanding of the pulsating jet is needed before any application can be performed. The need for this is to understand how the actuator will behave under different conditions and if there is any coupling between the actuating frequency and the jet velocity as it happens to acoustic actuators and other compact actuators. Moreover, we need to document how the asymmetry of the nozzle affects the profile.

The traversing scales, driven by stepper motors and controlled by the data-acquisition system, was used to orient the rake at positions along the leading edge slot, and perpendicular to the slot, seen in Figure 3-4. Velocity profiles were thus generated. We tested the actuator at supply pressures ranging from 40 psi to 100 psi and frequencies between 15 and 60 Hertz. A time record of the waveform for the steady state, as well as for pulsation obtained over the slotted nozzle is shown in Figure 3-1. For the same applied pressure of 80 psi the time records show that when the jet is pulsated it has a higher velocity than the steady jet. The RMS values of the two signals indicate a difference of almost 23 % increase from steady to a pulsating jet.

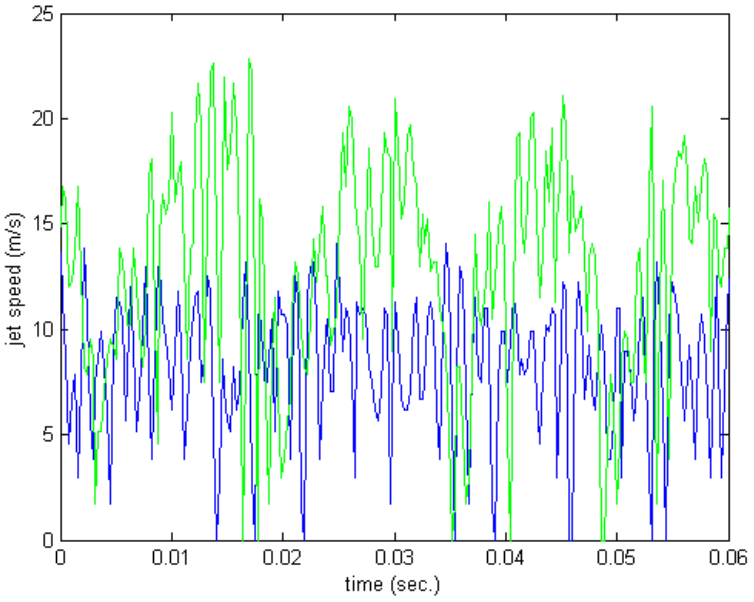

Figure 3-1: Time records for steady jet and for 63 Hz pulsating jet with the same pressure

Power spectra of such signals (in Figure 3-2) revealed that the dominant frequency of the jet was twice the driving frequency of the motor. The spectrum

confirmed that no motions were generated by nonlinear interactions, since the only other visible frequency was the second mode of the actuation frequency, and therefore this device could generate pulsed jets with any desired frequency within the limitations of the device, without introducing unwanted secondary frequencies. Named frequencies refer to the frequency of the jet, not the rotational frequency of the motor.

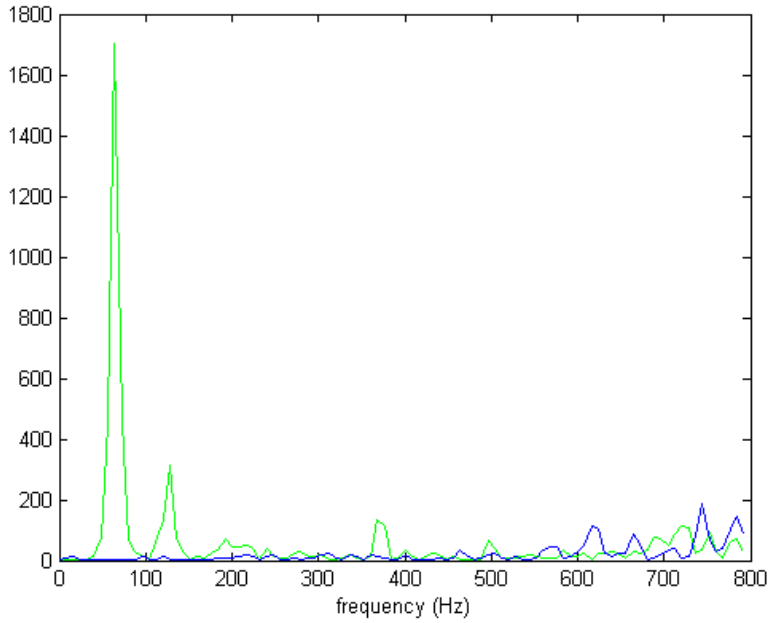

Figure 3-2: Power spectrum for steady jet and for 63 Hz pulsating jet with the same pressure

Another feature is that this actuator can produce pulsing jets with amplitudes independent of the driving frequency. We measured the velocities across the slot for a range of driving frequencies and for a fixed plenum pressure of 100 psig. The results are presented in Figure 3-3. These data indicate that the velocities generated by the device are almost completely independent of the driving frequency, and vary by up to 3.1% for data acquired at 100 psig driving pressure and down by 2.2 % for 25 psig and by 7.8% for 80 psig supply pressure. They remain fairly constant with some downward or flat trends as the frequencies are increased.

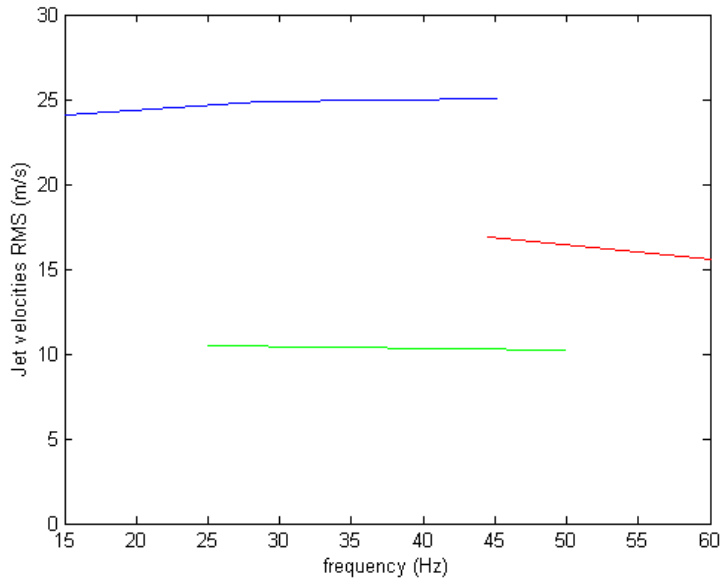

Figure 3-3: RMS for the jet speed at different pressures. Blue line is for 100 psig, red line is for 80 psig and green line is for 25 psig.

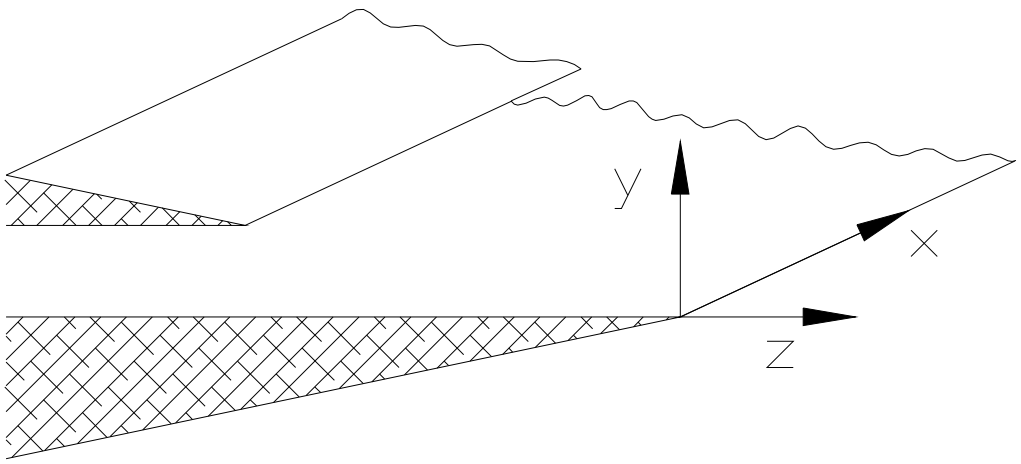

Figure 3-4: Sketch of coordinate system

Velocity profiles at different distances across the steady jet were also plotted in terms of coordinates laid out in Figure 3-4. In Figure 3-5 observed that the location of the maximum velocity is displaced upward, i.e. in the direction of the short side of the nozzle. This implies that there is a deviation of the direction of the jet away from the

direction of the z-axis of the duct as it moves in the outward direction of the edge. Averaged profiles for the pulsed jet are presented in Figure 3-6, Figure 3-7 and Figure 3-8 for three driving frequencies of 15, 29 and 45 Hz. In these three profiles, the vectoring of the jet is more pronounced although not by a high margin. This deviating tendency can be attributed to the asymmetry of the nozzle. As shown in Figure 3-4, one side of the jet duct is shorter than the other. As a result, the boundary layer on one side becomes a free shear layer before the other. Thus on one side, the free vorticity may start rolling, while the shear layer on the other side is constrained by the flat solid wall and vorticity retains its organization in the form of parallel flat layers. It is essentially a boundary layer. Rolled vortices may now generate regions of low pressure and thus induce changes in the direction of the jet. This is a Coanda effect. Apparently, this effect is mild for steady flow. This is expected, because the distance the free shear layer travels before the other side becomes free is short. For such a distance, no large vortical structures can grow. The situation is different with pulsing jet. An unsteady jet started from rest quickly rolls into two large vortices in two dimensions or a vortex ring in axisymmetric flow as suggested by Didden (1979) and Glezer (1998). In our case, the asymmetry of the two flat sidewalls allows the formation of a vortex on one side but forces vorticity to be confined in an attached boundary layer on the other side. The vortex being formed only on one side induces a low pressure as well as flow away from the long wall. A stronger vectoring away from the axis of symmetry of the wing and therefore a more effective disturbance will probably be introduced in the separated flow. In addition, the increase in frequency does not change further the velocity profiles with respect to the steady blowing case indicating that this further vectoring is a result of the pulsation without regard to magnitude of frequency.

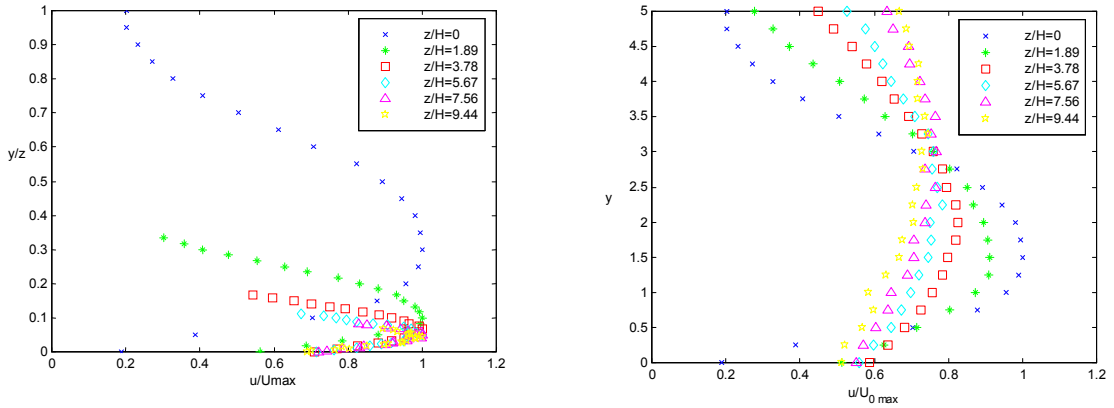

Figure 3-5: Actuator-jet velocity profiles in self-similar coordinates (left) and actual coordinates (right) Steady Blowing

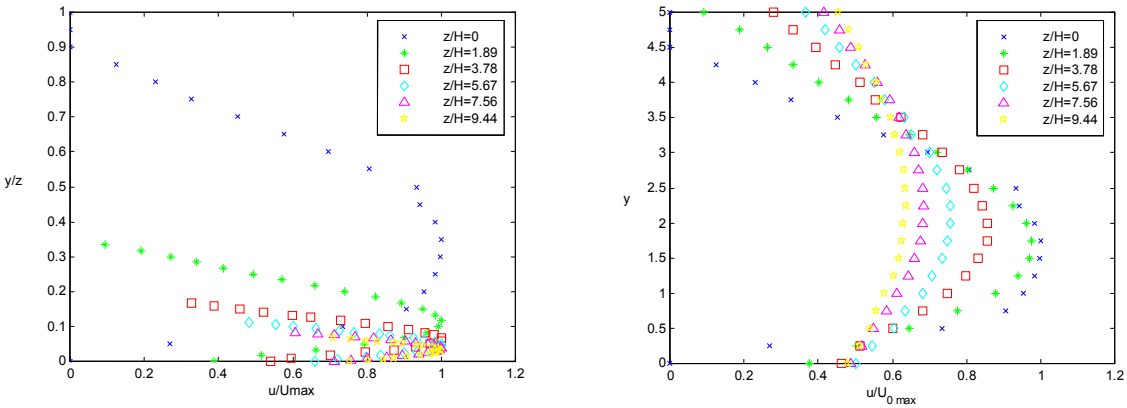

Figure 3-6: Actuator-jet velocity profiles in self-similar coordinates (left) and actual coordinates (right) 15 Hz

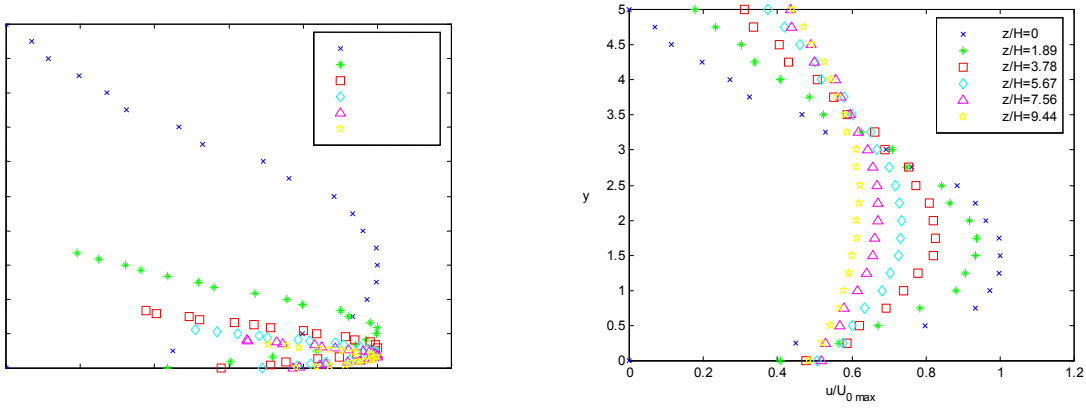

Figure 3-7 Actuator-jet velocity profiles in self-similar coordinates (left) and actual coordinates (right) 29 Hz

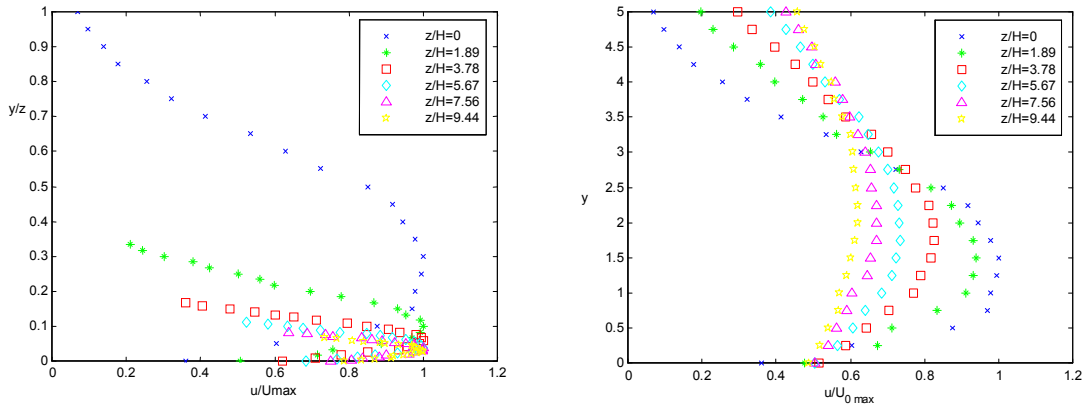

Figure 3-8: Actuator-jet velocity profiles in self-similar coordinates (left) and actual coordinates (right) 45 Hz

Water tunnel tests helped in documenting the development of the actuator jet and shed light on the asymmetry discussed above. A space resolution of 0.5 mm and temporal resolution of 1 millisecond was employed. Figure 3-9 shows a time sequence of 10 instantaneous velocity fields and vorticity distribution within one cycle of the actuator pulse. The frames are spaced apart by 0.02 secs. The initiation of the jet in the flow is shown in Figure 3-9-a. The formation of a pair of counter-rotating vortices continues in Figure 3-9-b. As discussed before, the slot geometry allows the generation of an asymmetric free-shear flow, confined in the lower side of the flow but allowed to accumulate vorticity and roll into a strong vortex in the upper side of the slot. This is better observed in Figures c-e where the clockwise vortex grows in strength as well as in size. As a result, it induces a velocity to the jet that favors the upper-side and effectively vectoring the jet at an angle with respect to the jet exit direction. At this point the dimensionless time is approximately t*=15 which means that the jet reaches a steady state condition. Thus, a jet parallel to the slot forms with the classic shear layer vortices illustrated in Figure 3-9f-i.

The important feature of this sequence is that the impulsive character of the jet favors the formation of a starting vortex on the upper side of the slot. This is equivalent to a passive control mechanism introduced by the slot geometry, inducing the jet to deviate at an angle with respect to the airfoil chord. This is a favorable feature, because when the jet interacts with the incident free stream, it curves and aligns itself better with the leading edge shear layer.

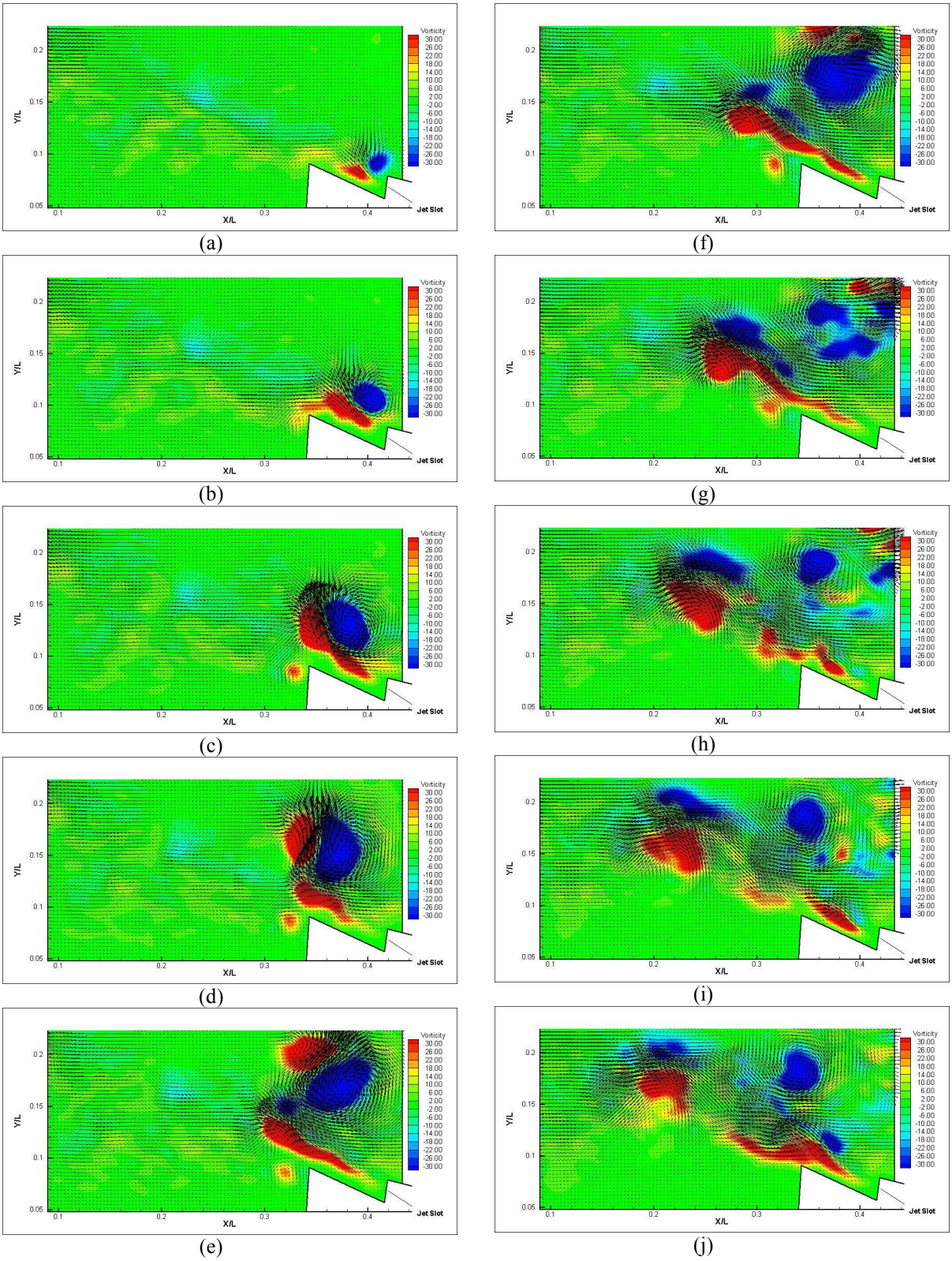

Figure 3-9: Time sequence of the actuator-jet vorticity contours and velocity distribution flow structure. t_{delay}=0.02 secs

The interaction and alignment with the leading edge shear layer can be observed in the following sequence of instantaneous flow fields. Figure 3-10-a and b show the separated shear layer before the initiation of the controlling pulsating jet. Clear shear layer instabilities are developing and the flow is highly disorganized. In Figure 3-10-c the initiation of the jet in the flow generates a clockwise rotating vortex with its locus approximately at x=0.13 y=0.1. This vortex induces a downward velocity to the shear layer vortices thus triggering a vortex pairing and the roll-up of a strong coherent vortex (Figure 3-10-c-d). In the subsequent figures (e-h), we witness one coherent vortex that interacts strongly with the airfoil increasing the vorticity (positive) levels and potentially inducing a pressure drop that will increase the suction and thus the lift. Remarkably, the dimensionless time required for vortex formation on the suction side is on the order of t*=15 which appears to be the same as the time required for the pulsing jet to reach a steady state. Figure 3-10-i-j demonstrates that as the strength of the pulsing jet decays, the strength of the suction vortex reduces.

The previous sequence of figures reveals the mechanism for controlling separated flow. The impulsively-started jet vortex interacts with the shear layer and its natural instabilities forcing these instabilities to grow through a vortex pairing process and subsequently forming a strong coherent vortex that increases the vorticity contribution. The continuation of the blowing within the pulsing cycle does not appear to further enhance the process. In contrast, the results indicate that the starting vortex is predominantly affecting the flow. This allows us to speculate that a more efficient way to manage the flow by minimizing the input would be by reducing the duty cycle of the pulsing for the same $C\mu$.

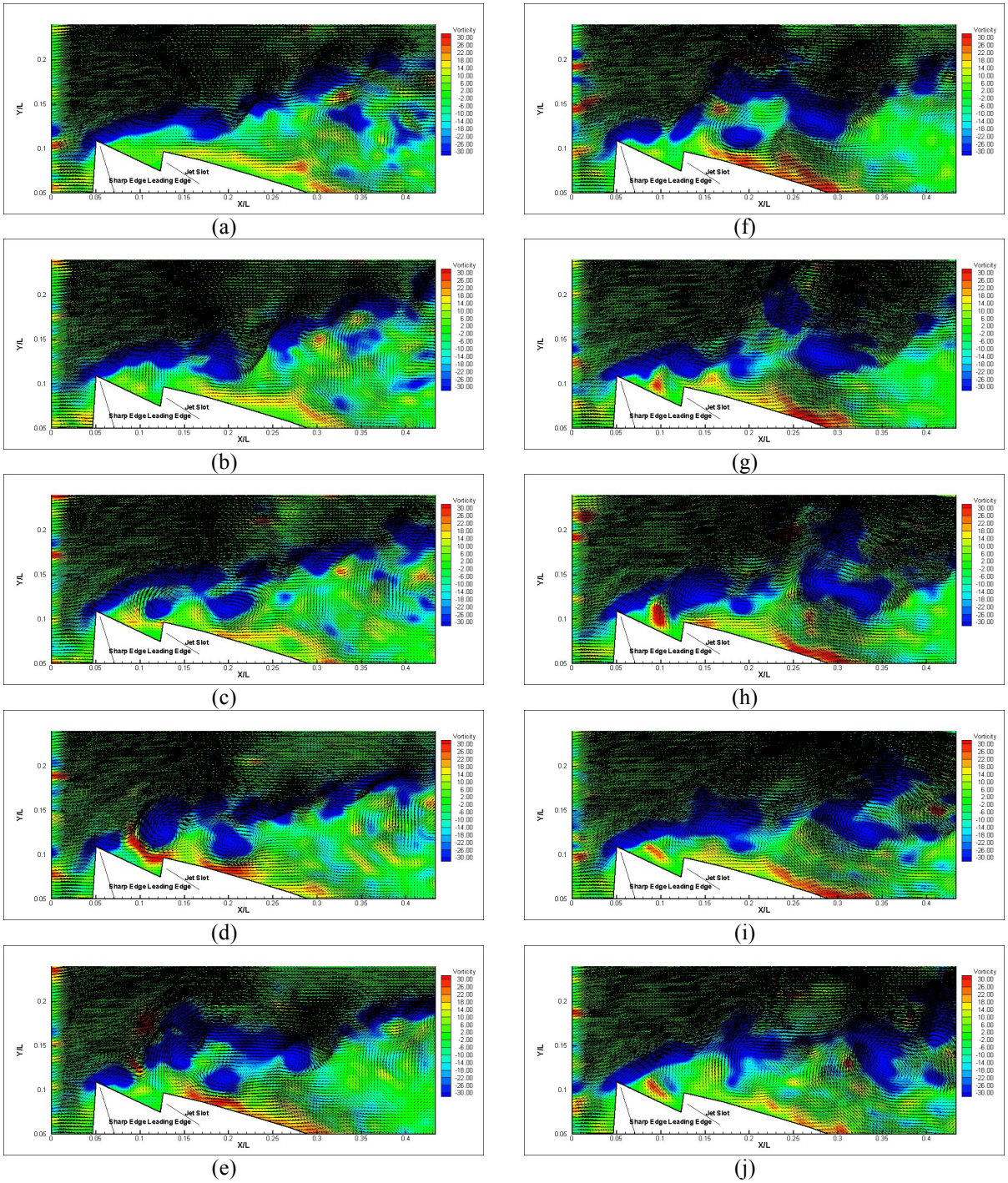

Figure 3-10: Time sequence of the controlled flow vorticity contours and velocity distribution

Our experimental data indicate that the velocity profiles generated by this actuator are nearly independent of the frequency. This means that the device is an excellent candidate for a robust flight actuator, where the required frequency and mass flow are changing with aircraft speed and the angle of attack. Another important feature of this device is that it can generate pulsing flow without any linearly oscillating parts, like a pulsating wall or piston. And due to the geometry of the nozzle the jet is going to have a tendency to be more aligned with the shear layer thus possibly reducing the energy needed.

4 PRESSURE DISTRIBUTION

We present the averaged pressure distributions over the suction and the pressure side of the airfoil for two different C_μ values and three angles of attack in the ESM wind tunnel. This setup had the problem that it suffered from solid blockage as defined by Pope et al (1999) since the model reduces the cross-sectional area of the tunnel, and as a result the air velocity around the model is increased. The model created a blockage of almost 21% when it was at 15° angle of attack. The results obtained in the ESM tunnel cannot provide direct information on lift and drag of sharp-edge wings. But our aim here is to explore the effects of flow control by comparing data obtained with and without control. The blowing amplitude was sustained at a constant level and the C_μ was adjusted by changing the free-stream velocity. The reduced frequency F^+ was changed and set at 0, 1, 1.5 and 2.

The pressure distributions do not indicate a clear stall situation for 10° (Figure 4-1) and even 15° and actually suggests attached flow in the average. For C_μ=0.0285 at α=15° (Figure 4-3) the control clearly increases the maximum suction. The suction strength is stronger on the leading edge part of the airfoil and it decreases towards the trailing edge. Unlike the other C_μ case that showed almost no improvement, here we observe a 15% drop in suction pressure. This difference suggests that the momentum coefficient C_μ should be at least greater than 1.5%. It also shows a small improvement when the actuator was operated at larger F^+ than unity. This indicates that the harmonics of the natural frequency get excited and can contribute to the resonance effect. One last observation from the second plot of each figure is that at smaller free stream speed (12 m/s and larger C_μ) the pressure distributions on the suction side for 10° (Figure 4-1), 15° (Figure 4-3), 20° (Figure 4-5) and somewhat for 25° (Figure 4-7) seem to be chaotic when there is no control. When control is applied, the chaotic situation is reduced or eliminated. This change in the profiles suggests that the actuation mechanism helps organizing the flow field for this particular situation of blockage.

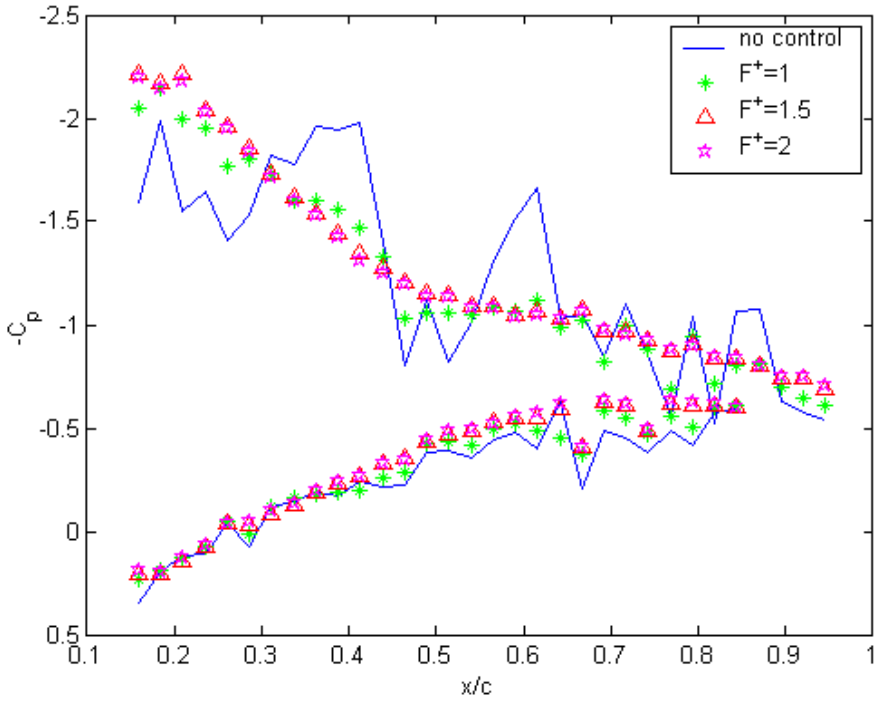

Figure 4-1: Averaged pressure distributions @ a=10° for Cμ=0.04

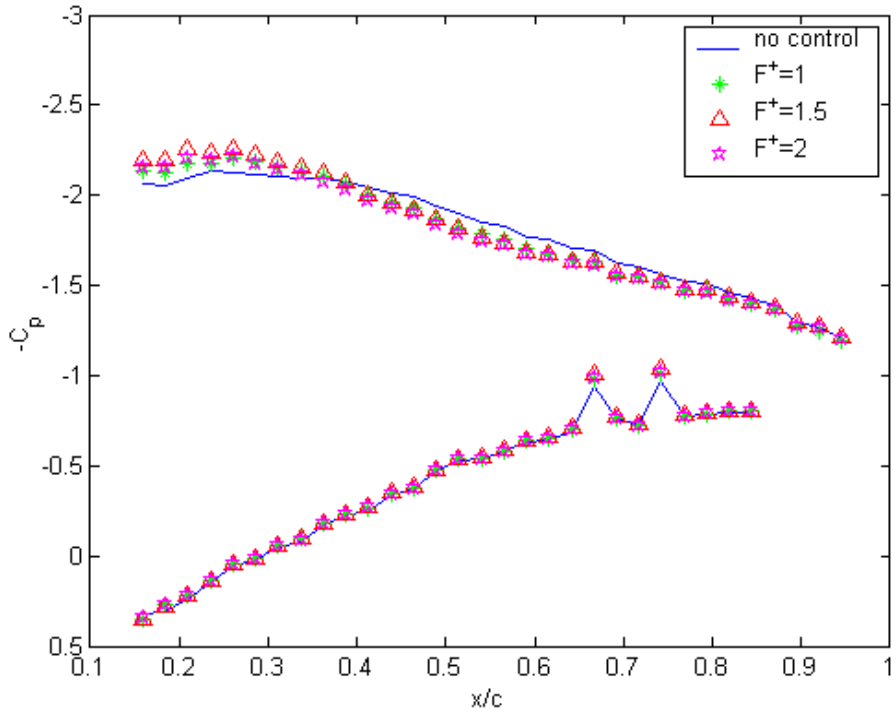

Figure 4-2: Averaged pressure distributions @ a=15° for Cμ=0.0171 for ESM wind tunnel.

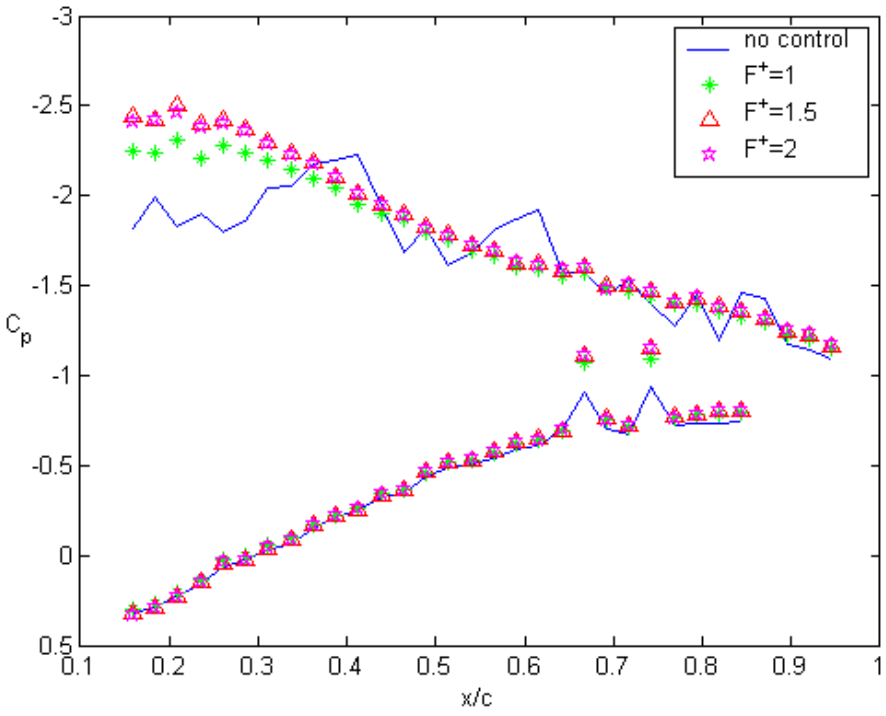

Figure 4-3: Averaged pressure distributions @ α=15° for Cμ=0.0285 for ESM wind tunnel.

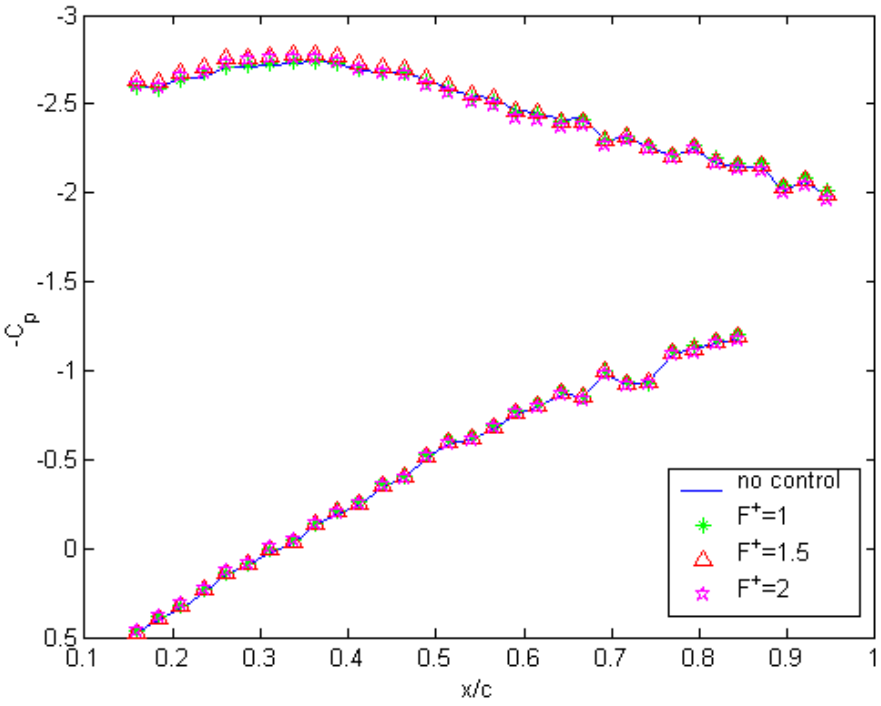

Figure 4-4: Averaged pressure distributions @ a=20° for Cμ=0.012991 for ESM wind tunnel

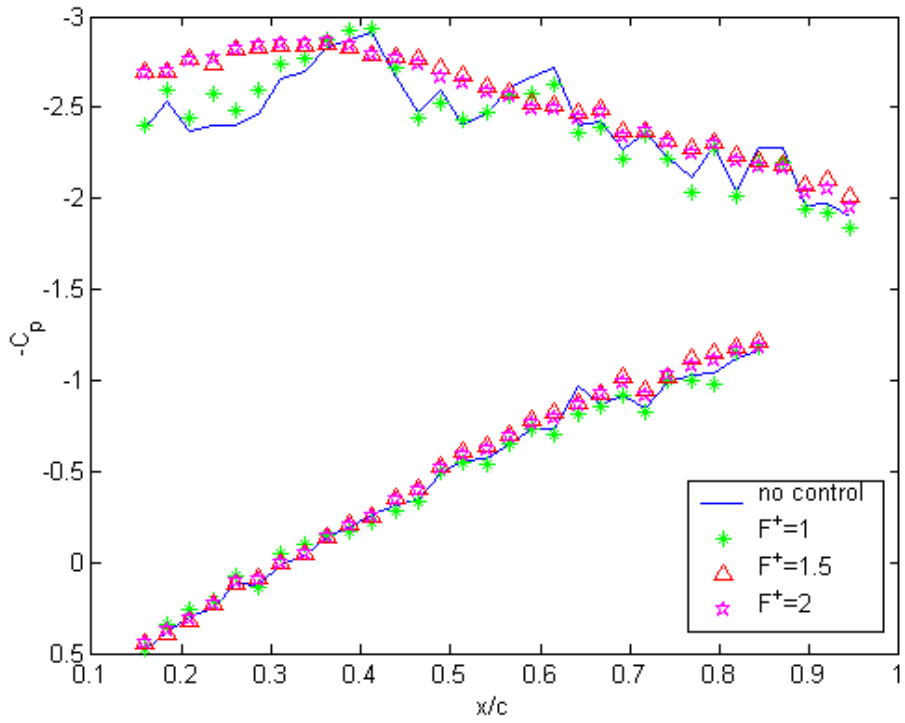

Figure 4-5: Averaged pressure distributions @ α=20° for Cμ=0.017321 for ESM wind tunnel

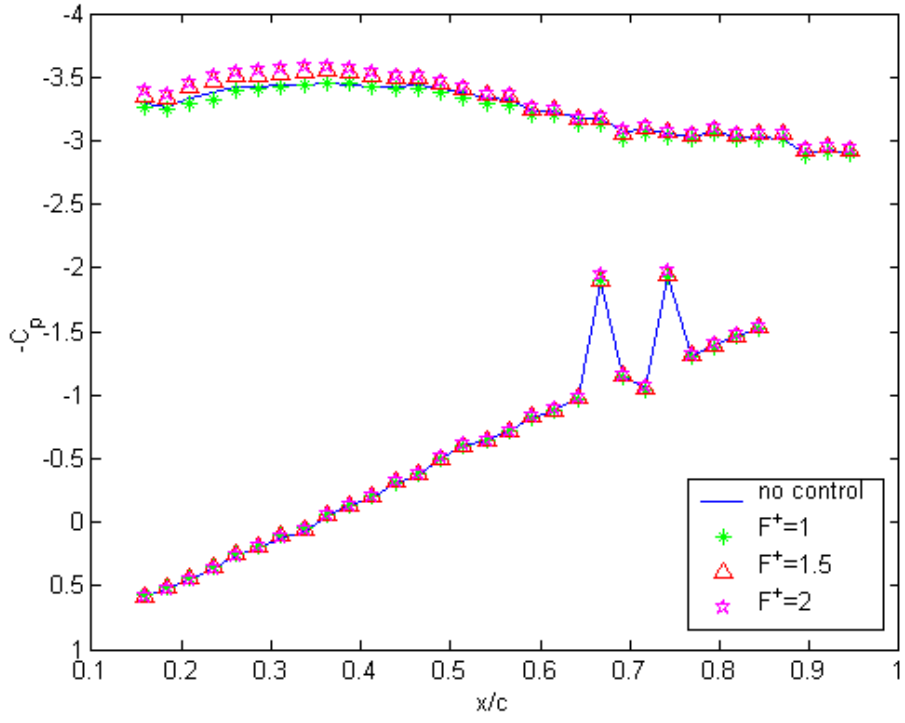

Figure 4-6: Averaged pressure distributions @ a=25° for Cμ=0.010513 for ESM wind tunnel

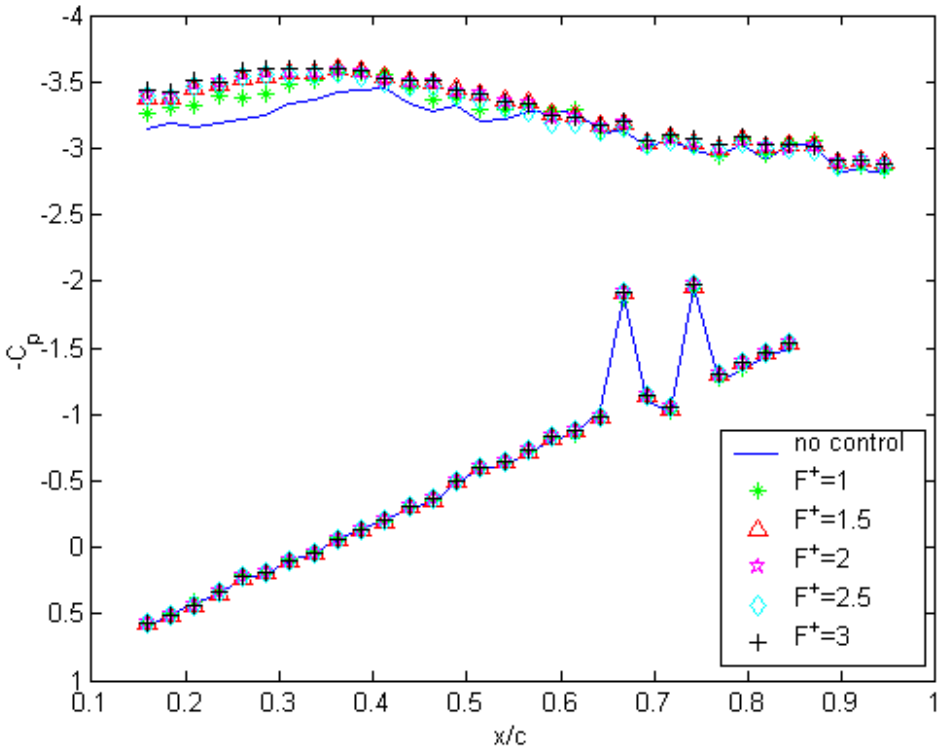

Figure 4-7: Averaged pressure distributions @ α=25° for Cμ=0.014018 for ESM wind tunnel

Tests were then carried out in the VA Tech Stability Wind Tunnel. In this tunnel, our model arrangement corresponds to a blockage coefficient 2.2% for an angle of attack of 21°. These tests can therefore simulate well the case of a wing in an infinite domain. The model was equipped with flat end plates to reduce as much as possible the end effects. This technique generates fields that are closer to two-dimensional motions than if the model were to be attached to the tunnel walls. The plates are better because boundary layers growing on the walls are thick and interact with the flow near the roots of the airfoil, giving rise to horseshoe vortices. Tests were carried out at angles of attack of 3° up to 21°, in increments of 3°. Also three different C_μ's were tried: 0.003, 0.01 and 0.03. Due to motor as well as air pressure supply limitations, the runs for the C_μ's were done at different tunnel speeds thus different Reynolds numbers. Figure 4-8 suggests that there is no Reynolds number dependence.

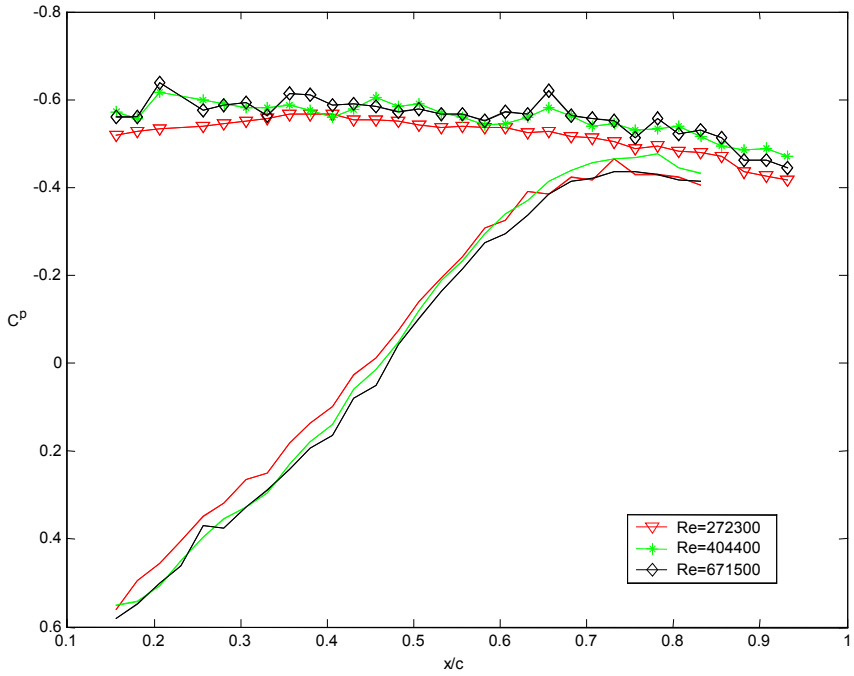

Figure 4-8: Averaged pressure distributions @ a=12° at different Reynolds number for the no control situation in the Stability wind tunnel.

Average pressure measurements for these angles of attack are shown in Figure 4-9 through Figure 4-15. For all these cases, the actuation frequency was set at the estimated value of the natural shedding frequency. It should be emphasized that because it was very difficult to place pressure taps on the leading edge wedge, we were not able to obtain pressure data very near the leading edge of the wing. For α=3° (Figure 4-9), there is a peculiar sharp drop near the leading edge on the suction side. We believe that this is due to a separated bubble very near the leading edge. Our control mechanism is not very effective at α=3° and 6°, a behavior we expected, since the flow is attached over most of our relatively thick wing. However, the control actuation lowers the pressure levels in the very front of the airfoil, where the separation bubble resides. The actuation is not effective even at α=9°, as shown in Figure 4-11. But at α=12° (Figure 4-12), we observe some significant departures from the no-control case. The comparison of the data of these two figures clearly indicates that the flow at α=9° displays the classical behavior of attached flow over airfoils. The suction pressure has its extreme values very near the leading edge. Suction is reduced as we move towards the trailing edge. But for $\alpha=12^0$, the

no-control case indicates a flat pressure distribution on the suction side. This is clear indication that the flow is massively separated. And yet, much like the case of oscillating mini-flaps, unsteady blowing at the leading edge brings the pressure distributions closer to those of attached flow, namely, the pressure is lowered near the leading edge and rises near the trailing edge. This is deceiving, because the flow is separated. It is only in the average that the pressure distribution is similar to the distribution of attached flow. The effect is more pronounced with higher levels of C_μ. In Figure 4-13, Figure 4-14 and Figure 4-15 ,α=15°, 18° and 21° respectively, the effect of flow control is not as large and in fact, it is progressively reduced as the angle of attack is increasing. It may be possible to achieve greater reductions on the suction pressure with larger values of C_μ, but due to limitations expressed before such tests could not be performed.

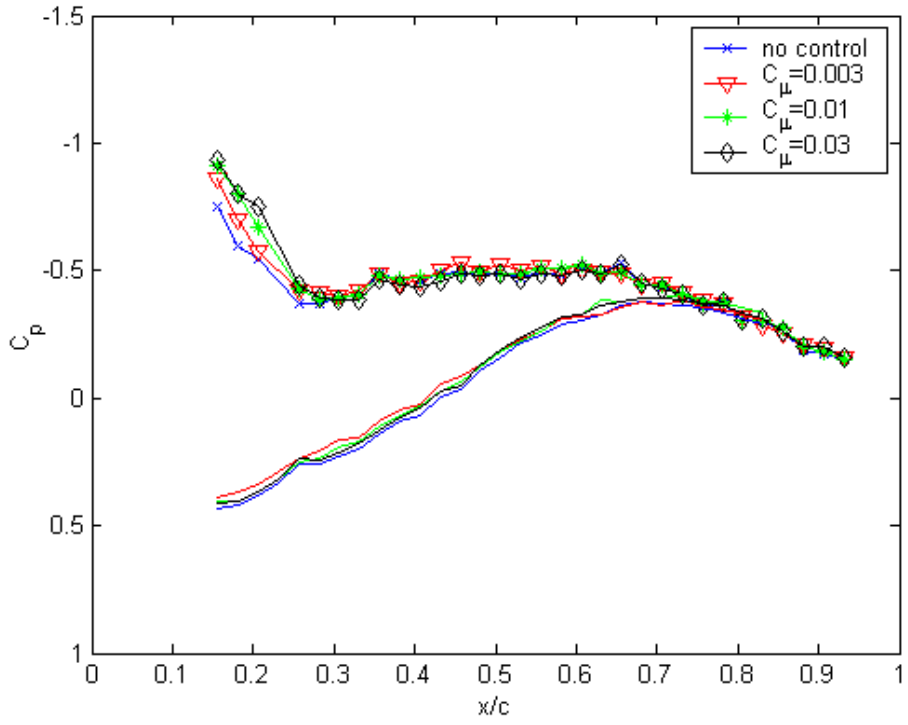

Figure 4-9: Averaged pressure distributions @ a=3° at Stability wind tunnel

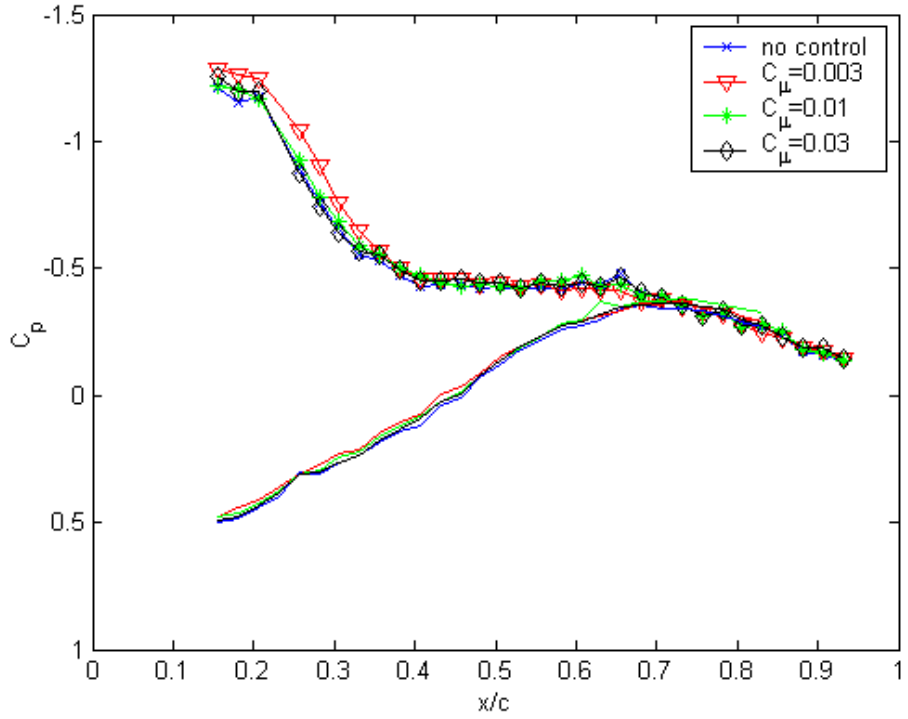

Figure 4-10: Averaged pressure distributions @ a=6° at Stability wind tunnel

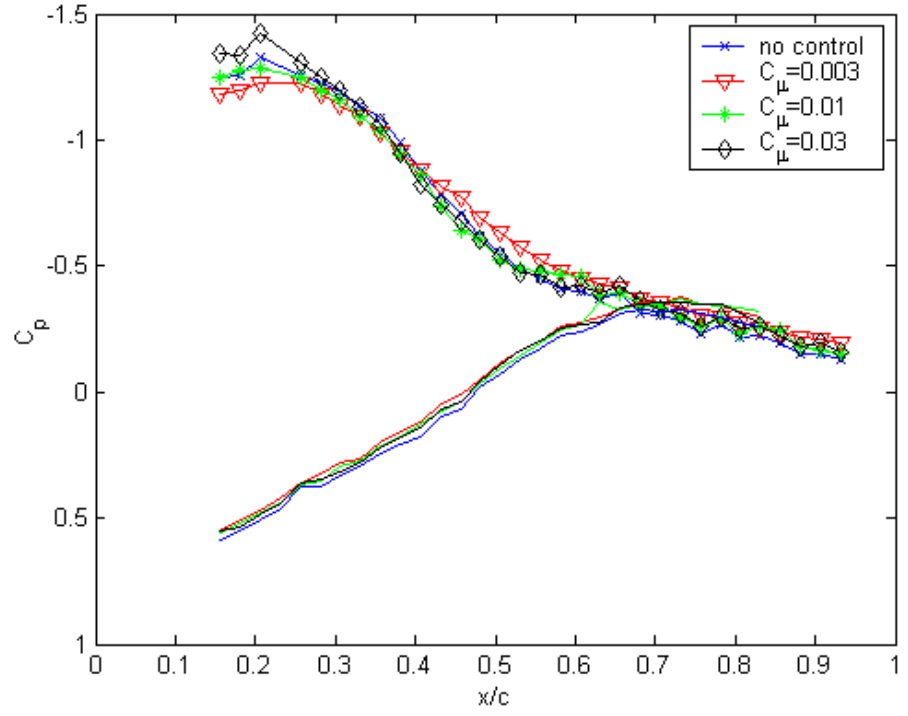

Figure 4-11: Averaged pressure distributions @ a=9° at Stability wind tunnel

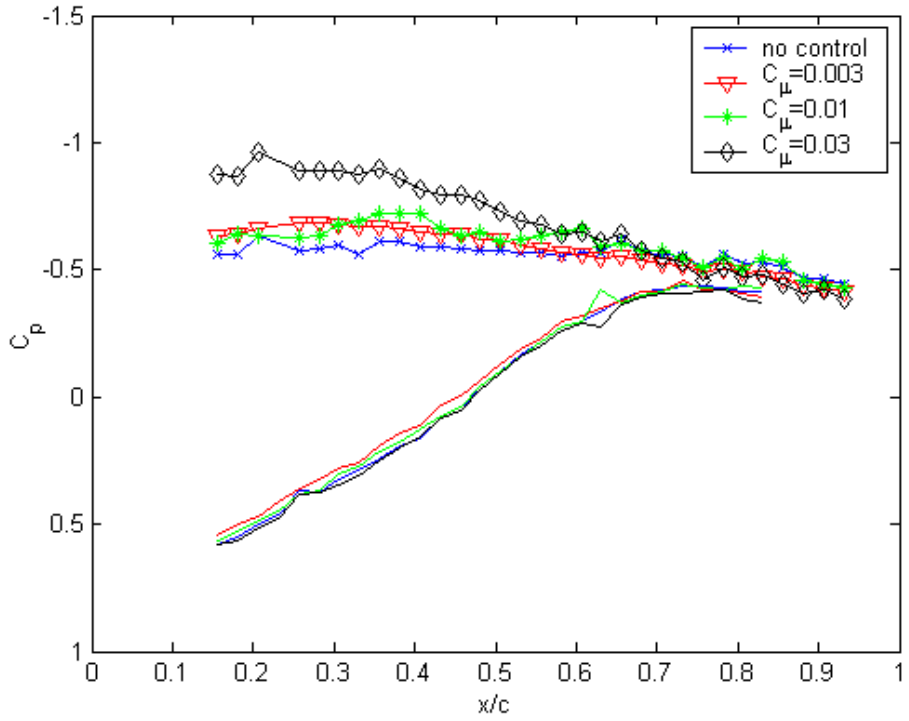

Figure 4-12: Averaged pressure distributions @ a=12° at Stability wind tunnel

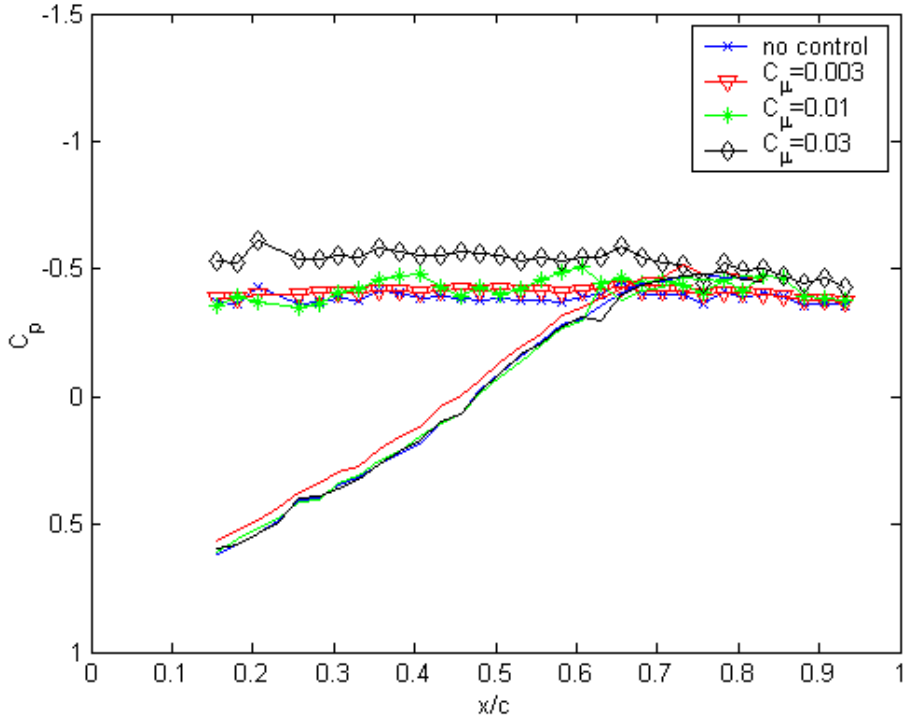

Figure 4-13: Averaged pressure distributions @ a=15° at Stability wind tunnel

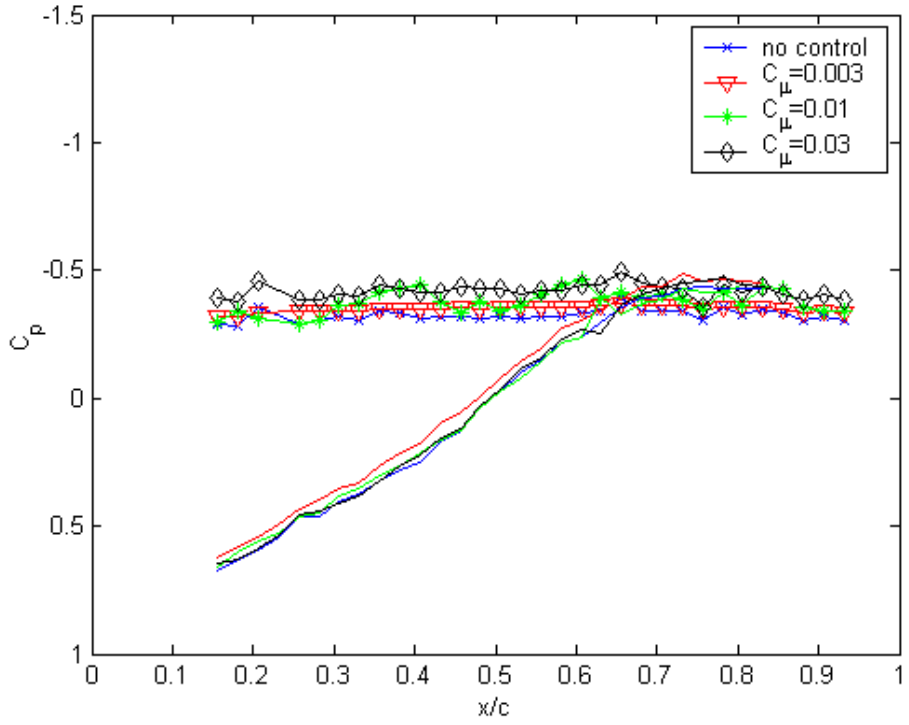

Figure 4-14: Averaged pressure distributions @ a=18° at Stability wind tunnel.

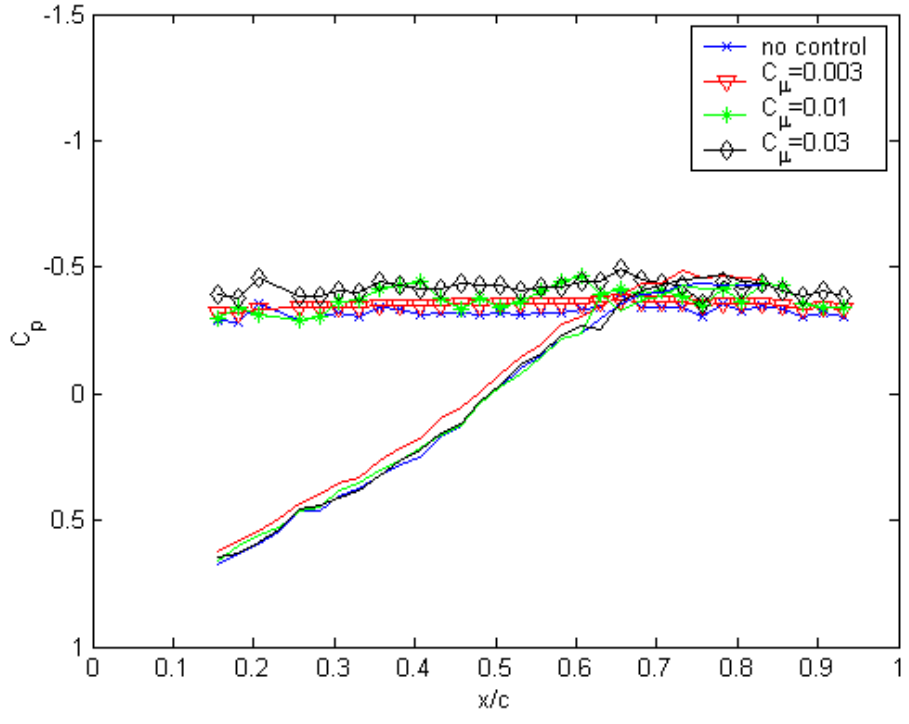

Figure 4-15: Averaged pressure distributions @ a=21° at Stability wind tunnel.

Lift coefficients were calculated by integrating the pressures over the suction and pressure sides of the wing. The results are presented in Table 1, for the three values of C_μ as well as no control. The benefit on the lift coefficient is large in the post stall area although it is reduced as is increased as seen in the last column, which is a comparison between the no control case and the control case with the highest C_μ. One of the reasons for this is that there were limitations in the actuating frequency. This suggests that even if it is not the natural frequency or one of its harmonics it is still possible to achieve some enhancement and increase the lift.

Table 1: Lift Coefficient C_L for conditions at Stability Tunnel

AOA	No control	C_μ = 0.003	C_μ= 0.01	C_μ= 0.03	Increase in C_L
3	0.4230	0.4150	0.4354	0.4458	5%
6	0.6420	0.6690	0.6277	0.6405	-0.23%
9	0.8410	0.8047	0.8046	0.8571	1.91%
12	0.5719	0.5905	0.6086	0.7344	28.41%
15	0.3881	0.3801	0.4131	0.5117	31.85%
18	0.3538	0.3424	0.3874	0.4395	24.22%
21	0.3618	0.3587	0.3884	0.4116	13.76%

The pattern previously discussed can be seen as well in Table 2, which describes the Lift to Drag ratio for the same conditions. Here the increase is not as pronounced as it is for the Lift coefficient. This indicates that the Drag is increasing as well. The vortex decreases the pressure over the surface but the force obtained is normal to the surface. When the angle of attack is increased the component of the normal force in the direction of the drag is increased as well and the lift component is reduced. This situation could be addressed by keeping the vortex closer to the front of the airfoil and detaching it farther from the trailing edge as the angle of attack is increased.

Table 2 : Lift to Drag ratio for conditions at Stability Tunnel

AOA	No control	C_μ = 0.003	C_μ= 0.01	C_μ= 0.03	Increase in C_L
3	7.2248	7.9616	8.0992	8.1356	12.6 %
6	9.3634	10.65213	9.2264	9.3714	2.8 %
9	7.5310	6.9529	7.1952	7.5868	0.74 %
12	3.0834	3.3201	3.1875	3.8473	24.77 %
15	2.1611	2.1575	2.1483	2.4982	15.60 %
18	1.8374	1.8156	1.8567	1.9781	7.65 %
21	1.6635	1.6381	1.6524	1.7168	3.20 %

It is emphasized that the data presented so far are averaged pressure distributions. Instantaneous pressure distributions over the wing at four specific instances are presented in Figure 4-16. These data provide evidence that large vortices are convected over the airfoil. In fact it is very possible that a dominant single vortex forms and convects, in the process inducing an imprint of a traveling wave of very low pressure. The first frame shows a dominant peak at about 0.4, while the last shows a new one and the previous one close to the end. This gives an approximate speed of propagation of the wave of 5.6 m/s at a U_∞=10 m/s, since the chord is .4064 m. This speed also shows that the wave frequency is 13.75 Hz while the power spectrum at x/c=0.48 shows two dominant frequencies: 13.4 Hz and 26.8 Hz. This corroborates the earlier estimate of the propagation frequency. It is important to note that power spectrum of signals from other ports showed no dominant frequency on port 28 and above meaning that the vortex probably detached from the surface at x/c=0.85. These spectra also showed that no frequency is defined in the first 2 ports. This suggests that the vortex does not form until x/c=0.2 and that a strong vortex convects over 65% of the suction side.

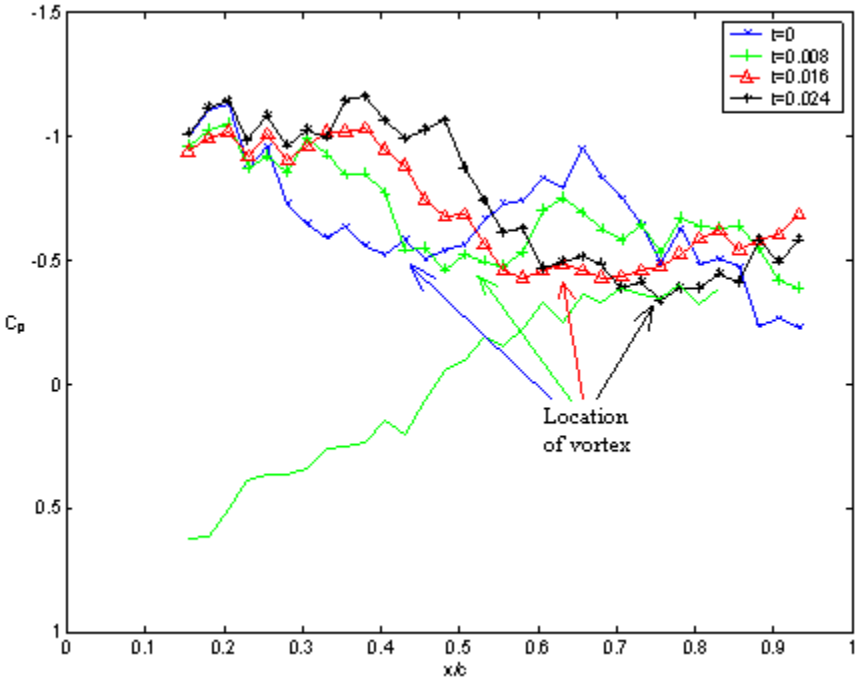

Figure 4-16: Wave propagation for α=12° with Cμ=0.03

It is useful to compare the data of Cahil et al (1953) with the present results although just for reference since their thickness coefficient was 0.06 and the current one is 0.12. Cahil et al. experimented with a circular arc airfoil equipped with leading and trailing edge flaps. Similar flaps are employed by aircrafts like the F-22, in order to increase lift during take off and landing. It is therefore very appropriate to compare the effect of a large leading edge flap, to the effects of flow control. Figure 4-17 shows that there exist agreement for pressure distributions at $\alpha=6^{\circ}$. In both cases the flow field is nearly attached. Near the leading edge the pressure distribution indicates that a separation bubble exists, effectively creating a virtual rounding of the leading edge. But at $\alpha=9^{0}$, the NACA data for no control indicates that the flow is fully separated, whereas the flow over our airfoil with no control appears to be still attached. This can be attributed to the wings' different thickness ratio. With only 6% thickness ratio the NACA airfoil is close to be a flat plate and thus at $\alpha=9^{\circ}$, the flow over such an airfoil is separated, displaying a nearly flat pressure distribution on the suction side. But with a thickness of 12% the flow over our airfoil stays attached. And for this reason, flow control does not provide any significant improvement. At $\alpha=12^{0}$ (Figure 4-19), the flow over the 12% airfoil is

separated as well. But now, flow control influences the flow field and thus the pressure distribution. It seems that the actuator can provide the necessary instability for these types of airfoils.

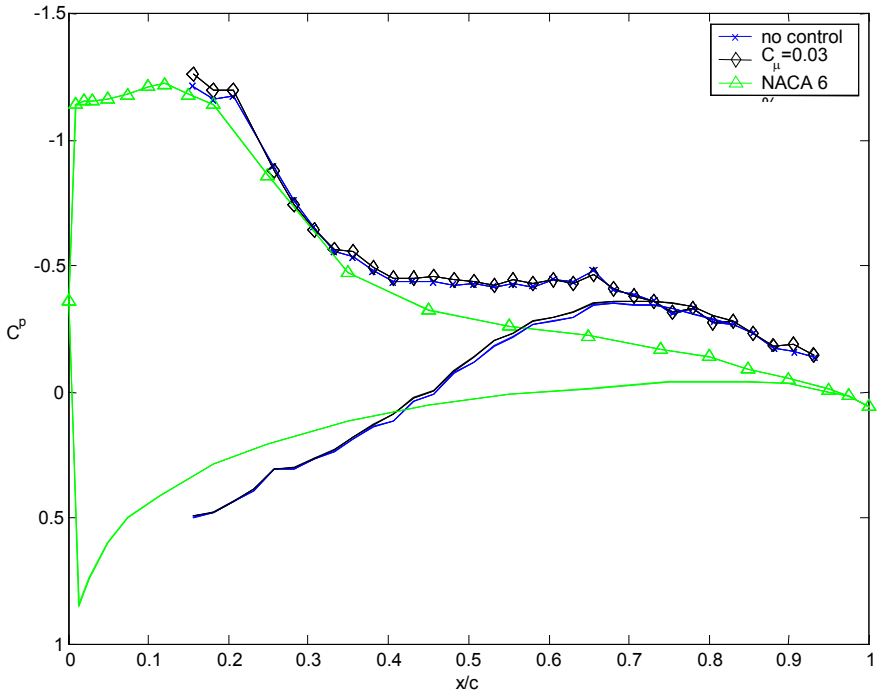

Figure 4-17: Comparison between NACA airfoil and Stability results @ α=6°

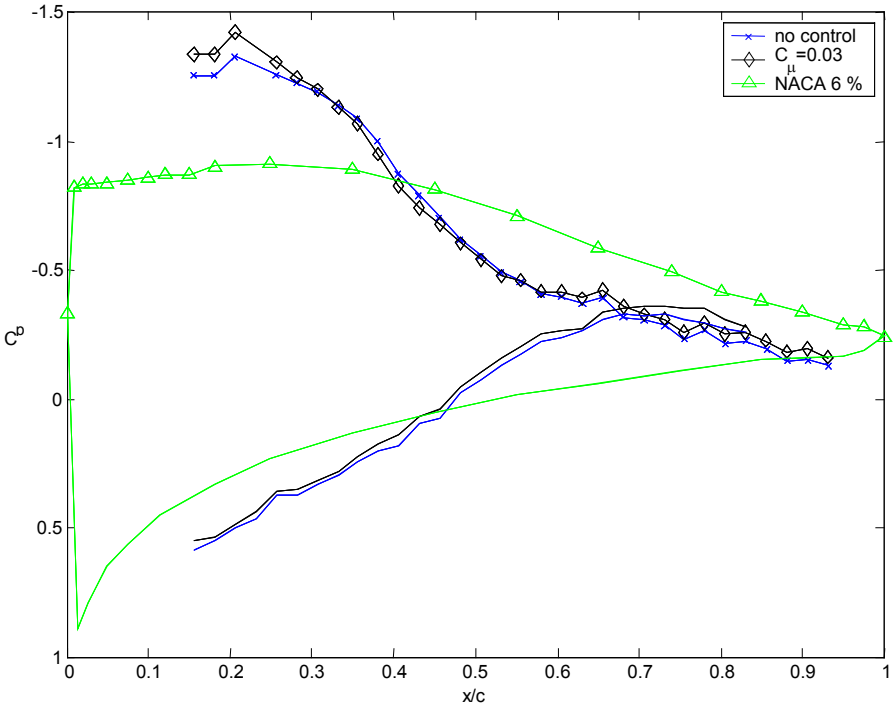

Figure 4-18: Comparison between NACA airfoil and Stability results @ a=9°

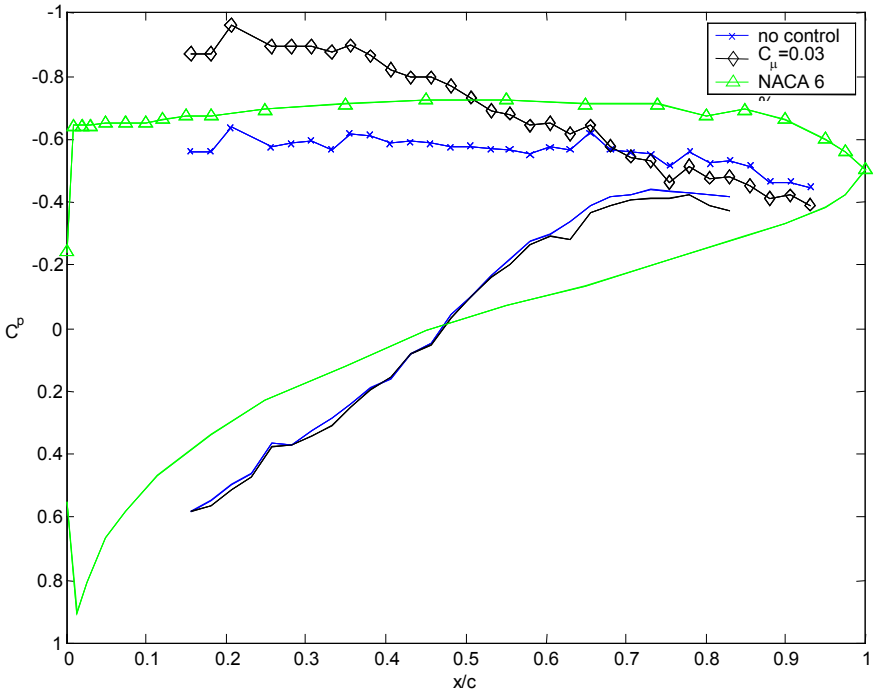

Figure 4-19: Comparison between NACA airfoil and Stability results @ a=12°

Finally, flow visualization over the entire airfoil was performed to document the global character of the flow. Time average streamlines and vorticity distributions are shown in Figure 4-20 for an α=15°, F+=1 and C_{μ}=0.02. Observing the two cases, uncontrolled (left) and the controlled (right), there is no radical differences between them. For both cases the flow is attached after the mid-chord. This may be due to the thickness of the airfoil (15%). The suction vortex appears to be more coherent and concentrated in the controlled case. Also, the trailing edge vortex is stronger, more defined and closer to the airfoil for the controlled case. This suggests that the leading edge vortex is stronger and more defined, since the interaction of the two vortices will bring them closer, be energized by the other and initiate the alternate vortex shedding pattern.

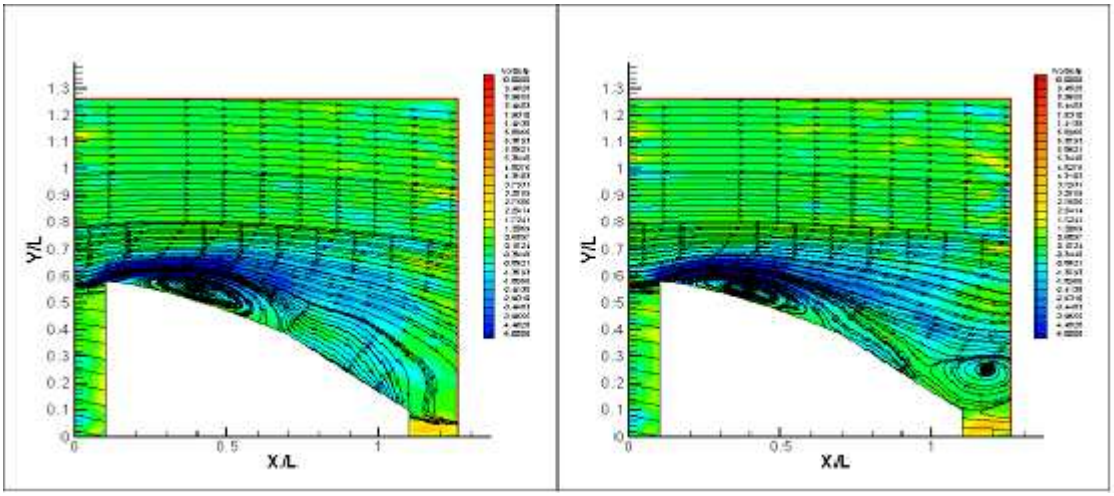

Figure 4-20: Time averaged streamlines and vorticity contours.
No control (left), control (right).

5 CONCLUSIONS

The purpose of this research was to develop a flow control mechanism that could generate a pulsing jet along a slotted nozzle to increase the lift of circular-arc airfoils. A novel pulsing jet actuator was designed and constructed. One of the features of this device is that it can generate oscillating disturbances without any mechanical parts like an oscillating flap, which could be detrimental to the radar signature of an airplane. Another feature is that the efficiency of this actuator is practically independent of the frequency. The design proved that uniform and more powerful pulsing jets could be generated along the span of the airfoil. In addition, this actuator did not generate nonlinear interactions and therefore any secondary frequencies as synthetic jets tend to do. This means that the device is an excellent candidate for a robust flight actuator, where the required frequency is changing with aircraft speed and angle of attack.

The location and geometry of the jet exit revealed that the asymmetry of the walls induces the formation of a starting vortex. This vortex provides a significant vectoring effect that guides the disturbance in the direction of the leading edge free shear layer. Moreover, this vortex interacts with the leading edge shear layer, exciting its natural instabilities and thus forcing the shear layer to roll, forming a strong coherent vortex.

Finally, we demonstrated for the first time, that unsteady blowing right at the leading edge of a sharp-edged circular arc airfoil allows the management of the separated flow, leading to averaged pressure distributions that correspond to higher lift. This was shown to be due to convecting vortices, as detected in the form of a low pressure traveling wave. Significant improvement was obtained in the lift coefficient for moderate to high angles of attack. But the effect decreased as the angle of attack was further increased, possibly due to less effective interaction between the disturbance and the shear layer. The data obtained with unsteady blowing indicate that there is a minimum of energy needed in order to exert a proper disturbance to the shear layer. In addition, the research suggests that the harmonics of the natural shedding frequency can have even greater impact than the natural frequency. Finally, the actuating frequency did not have to match the natural frequency since resonance was still achieved when locked to higher actuating frequencies.

Future work

A further review of the jet vectoring as well as an improvement of this vectoring is needed. In addition, understanding of the interactions of the possibly new direction of the disturbance is needed.

We need to address the issue of the control at different Reynolds numbers and find if different regimes affect the capacity of the actuator. We also need to study further the effects of different momentum as well as different reduced frequencies of the actuation jet. It is important to maximize the effect and minimize the energy consumption of this actuator to make it a feasible alternative to the flaps employed today.

Finally, a feedback mechanism that could detect the natural shedding frequency at any moment can help in locking the shedding frequency to the exact optimized actuation frequency.

REFERENCES

Abiven, C., Vlachos, P. P., (2002). "Super spatio-temporal resolution, digital PIV system for multi-phase flows with phase differentiation and simultaneous shape and size quantification", Int. Mech. Eng. Congress, Nov. 17-22, 2002, New Orleans, LA

Abiven, C., Vlachos P. P., Papadopoulos, G., (2002). "Comparative study of established DPIV algorithms for planar velocity measurements", Int. Mech. Eng. Congress, Nov. 17-22, 2002, New Orleans, LA

Amitay M, Smith B. L. and Glezer, (1998). "Aerodynamic flow control using synthetic jet technology", AIAA Paper 98-0208

Artana, G., D'Adamo, J., Léger, L., Moreau, E., Touchard, G., (2002). "Flow Control with Electrohydrodynamic Actuators" AIAA Journal Vol. 40, pp. 1773-1779

Cahill, J. F., Underwood, W.J., Nuber, R.J., Cheesman, G.A., (1953). "Aerodynamics forces on symmetrical circular-arc airfoils with plain leading-edge and plain trailing-edge flaps" NACA Report 1146

Cattafesta, L.N, Garg, S., Shukla, D., (2001). "Development of Piezoelectric Actuators for Active Flow Control". AIAA Journal Vol. 39, pp. 1562-1568

Didden, N. (1979). "On the Formation of Vortex Rings: Rolling Up and Productions of Circulation." Z. Angew. Math.Phys. Vol 30, pp101-106.

ELD, (1984) 24" Flow Visualization Water Tunnel, Operating and Maintenance Instructions

Fiedler, H. E., (1998). “Control of Free Turbulent Shear Flows”. In *Flow Control: Fundamentals and Practices* (ed. Gad-el-Hak, M., Pollard, A., Bonnet, J. P.), pp. 335-429

Gad-el-Hak , M., (2001). “Flow Control: the Future,” J. of Aircraft. Vol. 38, No. 3, pp. 402-418

Gilarranz, J. L., Rediniotis, O. K., (2001). “Compact, High-Power Synthetic Jet Actuators For Flow Separation Control,” AIAA Paper 2001-0737

Glezer, A. (1998): “The Formation of Vortex Rings”. Phys. Fluids, Vol 31, pp. 3532-3542.

Hsiao, F. –B., Wang, T.-Z., Zohar, Y., (1993). “Flow separation Control of a 2-D Airfoil by a Leading-Edge Oscillating Flap,” Intl. Conf. Aerospace Sci. Tech., Dec. 6-9, 1993, Tainan, Taiwan.

Hsiao, F. B., Liang, P. F., Huang, C. Y., (1998). “High-Incidence Airfoil Aerodynamics Improvement by Leading-edge Oscillating Flap”. J. of Aircraft. Vol. 35, No. 3, pp. 508-510.

Ho, C.-M. and Huerre, P. (1984) “Perturbed free shear layers”. Ann. Rev. Fluid Mech. 16, 365

Jacobson, S.A, Reynolds, W.C.,(1998), “Active Control of Streamwise Vortices and Streaks in Boundary Layers”, J. of Fluid Mechanics. Vol. 360, pp. 179-211.

McCormick, D. (2000), “Boundary Layer Separation Control with synthetic jets”, AIAA Paper 2000-0519

McManus, K., Magill, J., (1996). "Separation Control in Incompressible and Compressible Flows using Pulsed Jets". AIAA Paper 96-1948.

Miranda, S., Telionis, D., Zeiger, M., (2001). "Flow Control of a Sharp-Edged Airfoil", AIAA Paper No. 2001-0119, Jan. 2001

Pope, A., Barlow, J.B., Rae, W.H., *Low speed wind tunnel testing*, 3rd ed. p.353-356.

Prandtl, L. (1904) "Über Flüssigkeitbewegung bei sehr kleiner Reibung", Verhandlugen des III. Internatinalen Mathematiker-Kongres (Heidelberg) pp. 484-491, 1905

Rao, P. Gilarranz, J.L., Ko, J. Strgnac, T. and Rediniotis, O.K., (2000). "Flow Separation Control Via Synthetic Jet Actuation", AIAA Paper 2000-0407

Roshko, A., (1967), "A review of concepts in separated flow", Proceedings of Canadian Congress of Applied Mechanics, Vol. 1, 3-81 to 3-115

Scarano, F. and Rieuthmuller, M. L. (1999). "Iterative multigrid approach in PIV image processing with discrete window offset". Experiments in Fluids, 26, 513-523

Seifert, A., Bachar, T., Koss, D., Shepshelovich, M., Wygnanski, I. (1993). "Oscillatory Blowing: A Tool to Delay Boundary-Layer Separation". AIAA Journal. Vol. 31, No. 11, pp. 2052-2060.

Seifert, A., Pack, L.G., (1999). "Active Control of Separated Flows on Generic Configurations at High Reynolds Numbers". AIAA Paper 1999-3403

Smith B. L. and Glezer A., (1998). "The formation and evolution of synthetic jets". Phys. of Fluids 10, 2281-2297

Wereley S.T., Meinhart C.D. (2001). “Second-order accurate particle image velocimetry”. Experiments in Fluids, 31, pp. 258-268.

Wu, J.C., Vakili, A. D., Wu, J.M., (1991). “Review of the Physics of Enhancing Vortex Lift by Unsteady Excitation”, Prog. Aerospace Science, Vol. 28, pp. 73-131

Wu, J.M., Lu, X., Denny, A.G.,Fan, M. Wu, J.Z., (1997). “Post Stall Flow Control on an Airfoil by Local Unsteady Forcing”. Prog. AIAA Paper No 97-2063

Zeiger, M.D. and Telionis, D.P. (1997). “Effect of Coning Motion and Blowing on the Asymmetric Side Forces on a Slender Forbody”. AIAA Paper No 97-0549

Zeiger M. (2003). “The dynamic character of the flow over a 3.5 caliber tangent- ogive cylinder in steady and maneuvering states at high incidence”. Dissertation prepared for the Ph.D. Candidacy

Zhou, M. D., Fernholz, H. H., Ma, H. Y., Wu, J. Z., Wu, J. M., (1993). “Vortex Capture by a Two-Dimensional Airfoil with a Small Oscillating Leading-Edge Flap”. AIAA Paper 93-3266.

Zilliac, G.G., Degani, D. and Tobak, M. (1990). “Asymmetric Vortices on a Slender Body of Revolution”. AIAA Journal, pp 667-675

VITA

José Miguel Rullán was born in San Juan, Puerto Rico and raised in Utuado, Puerto Rico. He obtained a B.S. degree in Mechanical Engineering from the University of Puerto Rico in 1996. Upon graduation, he worked for a year at a family company as an Inspection Engineer where he oversaw the construction of a school and a fire station. Looking for new challenges he moved to Phillips Puerto Rico Core, a chemical plant, to work as Project Engineer. There he performed tasks related to project development, from design to completion. In 2000 he moved to Blacksburg, Virginia for graduate school, and in 2004 she obtained an M.S. degree in Engineering Mechanics with a concentration in fluid mechanics from the Department of Engineering Science and Mechanics at Virginia Polytechnic Institute and State University. During his master's studies he served as a graduate teaching assistant that provided a great experience in the educational arena. Mr. Rullán is a licensed Professional Engineer in Puerto Rico and is a member of the College of Professional Engineers and Land Surveyors of Puerto Rico and the American Institute of Aerospace and Aeronautics. Mr. Rullán currently lives with his wife and son in Blacksburg, Virginia.